The clays involved in the 1963 Vajont landslide: Genesis and geomechanical implications

PAOLO PARONUZZI[1], ALBERTO BOLLA[1]*, DANIELA PINTO[2],
DAVIDE LENAZ[3], MASSIMO SOCCAL[1]

[1] Dipartimento Politecnico di Ingegneria e Architettura, Università degli Studi di Udine, via Cotonificio 114 – 33100 Udine, Italy

[2] Dipartimento di Scienze della Terra e Geoambientali, Università degli Studi di Bari A. Moro, via Orabona 4 – 70125 Bari, Italy

[3] Dipartimento di Matematica e Geoscienze, Università degli Studi di Trieste, via Weiss 8 – 34127 Trieste, Italy

* Corresponding author. Tel.: +39 0432-558738; Fax: +39 0432-558700; E-mail: alberto.bolla@uniud.it

Abstract

The catastrophic Vajont landslide that occurred on 9 October 1963 caused about 2,000 deaths when 270–300 Mm^3 of rock and debris slid from the northern slope of Mt. Toc into the newly created artificial reservoir, displacing some huge water waves that flooded the nearby villages. The 1963 slide was an en-block remobilisation of a prehistoric rockslide lying on the southern reservoir bank. Basal sliding took place within a complex lithostratigraphic sequence of cherty–marly limestones and clay

interbeds belonging to the Fonzaso Formation of Upper Jurassic age. In this work, we investigate the geological origin and provenance of the Vajont clays according to the results of mineralogical and geochemical analyses performed on several clay samples which were collected from the landslide failure surface and the same limestone sequence in the surrounding area. The sampled clayey materials contained variable amounts of clay minerals (36–96%), calcite (4–64%) and quartz (0–6%). The dominant clay minerals were illite/smectite (I/S) mixed layers with a high illite content (85–50%), which was consistent with the high percentage of K_2O (1.17–5.77%). The Vajont clays included in the Fonzaso Fm. can be referred to as K-bentonites and can be interpreted as distinct deposits of volcanoclastic materials (tephra), representing the sedimentary inputs of volcanic ashes that interrupted the "normal" calcareous sedimentation during the late Oxfordian–upper Tithonian (158–145 Ma). The soft clay interbeds played a different mechanical role in the occurrence of the prehistoric rockslide and the 1963 en-block remobilisation. Distinct clay-rich layers that were concentrated within some specific lithostratigraphic intervals of the Jurassic cherty limestone sequence caused a localised decrease in the available shear strength, allowing for relative shear displacements along the dip-slope bedding planes. This caused additional shear/tensile fracturing of limestone beds and the formation of a stepped basal failure surface. During the 1963 remobilisation, the clay layers contributed in the average shear strength decrease of the debris material forming the basal shear zone of the slide, but the main triggering factor was the increase in pore pressures caused by the reservoir-induced groundwater inflow.

Keywords: Vajont landslide; Clay; Illite/Smectite mixed layer; Shear strength; Volcanic ash; Jurassic tephra

1. Introduction

The 270–300 Mm^3 Vajont landslide (Fig. 1) was and still remains one of the largest mass movements in the Alps (Müller, 1964; Paronuzzi et al., 2013a). This catastrophic landslide occurred in the Vajont valley, in the South-eastern Alps, in the Friuli Venezia Giulia Region, about 120 km north to Venice (Italy). The Vajont valley is a prevailing E–W trend fluvio-glacial valley crossed by the homonymous stream, a tributary of the Piave river, which was dammed to construct a hydroelectric power plant. The 261.60 m-height concrete double-curvature arch dam was constructed between 1957 and 1960 in the narrow Vajont gorge eroded in the oolitic limestone of the Calcare del Vajont Formation of Middle Jurassic age and was the tallest dam in the world at that time (today, the 7th). On 9 October 1963, as a result of the three filling–drawdown cycles of the Vajont reservoir (Paronuzzi et al., 2016), a huge rock mass detached from the northern slope of Mt. Toc on the southern valley flank and slid as a coherent block into the reservoir. As Fig. 1 shows, the dam survived the impact, but the failed mass generated a number of waves that caused massive flooding and the complete destruction of towns and villages, provoking the deaths of about 2,000 people. On 12 February 2008, when launching the International Year of Planet Earth, the United Nations Educational, Scientific and Cultural Organization (UNESCO) cited the 1963 Vajont landslide as the worst man-made environmental disaster of all time (https://en.lswn.it/events/international-year-of-planet-earth-global-launch-event-12-13-february-2008/).

The causes of the 1963 Vajont landslide have to be related to both predisposing and triggering factors. A large number of studies agree on identifying as predisposing geological factors for the large slope failure the general attitude of the dip-slope bedding planes, the presence of soft clay interbeds within the thinly stratified limestone sequence

of the Fonzaso Formation of Upper Jurassic age that was involved in the basal failure, and the presence of some major faults representing lateral and rear release surfaces (e.g., Selli and Trevisan, 1964; Hendron and Patton, 1985; Paronuzzi and Bolla, 2012, 2015a; Wolter et al., 2014). The existence of a prehistoric rockslide lying on the northern slope of Mt. Toc was also widely recognised as a determining factor for the occurrence of the 1963 Vajont slide, since the failure surface was pre-determined and the materials involved in the basal sliding were at their residual shear strength (Hendron and Patton, 1985; Kenney, 1992; Alonso and Pinyol, 2010; Paronuzzi and Bolla, 2016). However, it must also be noted that, based on geomorphological or geotechnical considerations, some authors still dispute the occurrence of the prehistoric rockslide (Wolter et al., 2016; Dykes and Bromhead, 2018).

When considering other possible geological factors that favoured slope instability processes at Vajont, Skempton (1966) addressed folding of the layered sequence that gave rise to bedding plane slip occurring in weaker clayey beds, thus reducing strength to near residual values between more rigid limestone beds. Mantovani and Vita-Finzi (2003) advanced the hypothesis that the slide surface was an exhumed fault plane, with the slide material composed predominantly of fault gauge. Kiersch (1964), Lo et al. (1972) and Hendron and Patton (1985) also speculated on the probable existence of artesian pressures acting along the base of the slide due to karst in the underlying oolitic limestone of the Calcare del Vajont Formation, which may have originated a rapid rise of groundwater levels due to rainfall.

In addition, as demonstrated by extensive field evidence (Paronuzzi and Bolla, 2012, 2015a), a decisive geological factor contributing to the 1963 slide was the occurrence of a 40 m-thick shear zone at the base of the unstable slope. The basal shear zone was characterised by a chaotic assemblage of highly permeable limestone angular

gravel, displaced and fractured rock masses, and spread clay lenses with high plasticity and very low residual shear strength (Paronuzzi et al., 2013a, b; Bolla et al., 2020). The debris material forming the basal shear zone was the result of the disintegration of the primary rock mass at the base of the prehistoric rockslide during the ancient slide propagation (Paronuzzi and Bolla, 2015a). The presence of this "debris cushion" at the base of the 1963 slide was extremely unfavourable for slope stability owing to the combined poor mechanical properties of clay beds and the high permeability of the angular limestone gravel, which determined a rapid reservoir-induced inflow. Moreover, the ductile shear zone at the base of the slide favoured the en-block motion of the 1963 catastrophic collapse (Fig. 1).

Besides the aforementioned predisposing factors, the main trigger of the 1963 Vajont landslide was the adjacent reservoir at the toe of Mt. Toc slope, which caused the formation of a water table within the highly permeable debris material of the basal shear zone, thus inducing a decrease in the overall shear strength along the failure surface (Paronuzzi et al., 2013a, 2016). According to their hypothesis for the presence of an artesian aquifer beneath the main failure surface, Hendron and Patton (1985) asserted that the Vajont landslide would have occurred even in the absence of the reservoir and as a result of periods of heavy or prolonged rainfall. However, on the basis of some stability analyses of the northern slope of Mt. Toc, Paronuzzi et al. (2013a) demonstrated that only precipitation would not have been able to lead the slope to the collapse. This means that the catastrophic 1963 slope failure could have been avoided if no reservoir had been constructed in the Vajont valley.

Although the presence of clay interbeds within the rock mass involved in the slope rupture is considered as a determining factor in the occurrence of the catastrophic collapse, some issues still need to be addressed. In particular, the geological origin and

126 the related provenance of the Vajont clays has never been investigated. In addition, the
127 mechanical role played by the clay layers in both the ancient rockslide and the 1963
128 reactivation has not been fully understood in relation to the mineralogy, geotechnical
129 properties, lenticular shape and lithostratigraphic position of the clay beds. These issues
130 will be discussed in the present paper on the basis of additional geological field
131 observations, new geochemical data on trace elements of the sampled clayey materials
132 and further considerations on geological and mineralogical features of the Vajont clays
133 along with their geomechanical implications in the repeated instability processes that
134 occurred on the northern slope of Mt. Toc.
135
136 **2. Previous investigations on the Vajont clays**
137 Despite the occurrence of clay layers within the layered sequence of the Fonzaso
138 Formation at the base of the slide is now widely accepted, this topic was controversial
139 for decades after the catastrophic event. As a result of the survey of the failure scar,
140 Broili (1967) stated that the lithostratigraphic sequence involved in the rupture did not
141 include any clay layers, although very thin 1–3 mm-thick interbeds of limey marl and
142 marly limestone were present. X-ray diffraction analyses revealed these pelitic beds
143 contained an average of 16% montmorillonite and probably illite clay minerals (Broili,
144 1967), as shown here in Table 1. However, studies by Kenney (1967) and Nonveiller
145 (1967) reported the laboratory results on the mineralogical composition and residual
146 shear strength properties of some clay samples collected from the basal failure surface
147 of the Vajont slide (Table 1). In particular, the first semi-quantitative determinations
148 performed via X-ray diffraction on the Vajont clays revealed a content of 25–75%
149 montmorillonite that resulted in low values of the residual angle of internal friction,
150 which was found to be strongly dependant on the system chemistry (Kenney, 1967).

151 This evidence was disputed by Müller (1968), who contended that clayey beds in the
152 strict sense, would not be present in a limestone sequence dated to Jurassic, inferring the
153 presence of claystone interbeds, on the basis of Broili's (1967) interpretation. It must be
154 noted that the lithostratigraphic sequence involved in the slope failure was not fully
155 known at that time, and Müller's opinion was based on his knowledge of the geological
156 aspects referred to the Jurassic age.

157 The debated question of clay interbeds was definitively resolved thanks to the
158 detailed geological survey carried out on the failure surface some years later by
159 Hendron and Patton (1985): several plastic clay layers were sampled, intercalated within
160 the cherty limestone bedrock (Fig. 2) as well as mixed with uncemented angular gravel
161 and sand-sized breccia forming debris strips resting on the basal detachment plane of
162 the slide. However, the origin of this debris material was not clearly established by
163 Hendron and Patton (1985), who supposed that it may have been the result of landslide
164 processes (Hendron and Patton, 1985; p. 26). The clay mineral analyses pointed out the
165 presence of 50–80% Ca-montmorillonite and some vermiculite/smectite mixed layers
166 for the first time (Hendron and Patton, 1985; Table 1). Some residual shear strength
167 tests on the sampled clayey materials revealed very low resistance properties, with
168 values of the residual friction angle varying between 5° and 16°. Hendron and Patton
169 also argued that the failure surface of the 1963 slide coincided with "one or more clay
170 layers which were continuous over large areas of the surface of sliding" (Hendron and
171 Patton, 1985; p. 91).

172 However, field observations carried out on the large failure surface demonstrated
173 that the latter was not flat, and differently, was characterised by a marked stepped
174 morphology (Broili, 1967; Paronuzzi and Bolla, 2012, 2015a; Wolter et al., 2014). In
175 fact, the outcropping failure surface mainly follows the extended bedding planes, but

176 also includes multiple steps coinciding with high-angle cross-cutting joints that expose
177 different layers of the limestone sequence involved in the rupture, with directions that
178 are both parallel and sub-orthogonal to the slide movement (Paronuzzi and Bolla,
179 2015a). It must also be noted that, owing to the large extent of the exposed failure
180 surface (about 1 km^2), its average dip is very close to the dip of the bedding planes, i.e.
181 34° in the western sector and 44° in the eastern sector (Paronuzzi and Bolla, 2012).
182 Investigations on mineralogical and strength properties of Vajont clays were also
183 carried out in order to determine values of the friction coefficient that can explain the
184 dynamic features of the landslide (Tika and Hutchinson, 1999; Ferri et al., 2011). In
185 particular, Tika and Hutchinson (1999) proved the copious existence of illite/smectite
186 mixed layers in the clay mineral mixtures occurring within the rock mass involved in
187 the slope failure (Table 1). Ferri et al. (2011) investigated the frictional properties of a
188 single 60–70% smectite-rich sample from the Vajont slipping zone under presumably
189 similar conditions as during the landslide: 1–5 MPa normal stress, 2×10^{-7} to 1.31 m/s
190 slip rate, displacements up to 34 m and variable water content from 40–60% up to
191 saturation. The frictional properties of the clay-rich sample were found to decrease as
192 both the velocity and water content increase, owing to thermo-chemical pressurization
193 of pore fluids and powder lubrication (Ferri et al., 2011).
194 In a recent paper (Bolla et al., 2020), mineralogical investigations on clayey
195 materials sampled from the Vajont slide showed the occurrence of illite/smectite mixed
196 layers as dominant clay mineral phases along with variable amounts of calcite and low
197 quartz percentages (Table 1). The residual shear tests demonstrated, for the first time,
198 highly variable shear resistance properties of the clay interbeds. Indeed, samples with a
199 large prevalence of clay minerals (CM > 79%) were characterised by low values of the
200 residual angle of internal friction (7–15°), whereas clayey materials characterised by a

higher content of granular minerals (calcite and quartz) showed greater values of the residual friction angle (20–27°).

3. Materials and methods

3.1. Fieldwork and sampling

Previous field surveys performed by the Authors on the 1963 Vajont slide were aimed at identifying and sampling clayey materials occurring within the rock mass involved in the slope failure (Paronuzzi and Bolla, 2012, 2013, 2015a). Bolla et al. (2020) subsequently reported the first results of laboratory investigations on the chemical and mineralogical composition of the Vajont clays, which was determined through major oxide X-ray Fluorescence (XRF) and semi-quantitative X-ray Powder Diffraction (XRPD) analyses, along with their geotechnical properties. In the present paper, a more detailed analysis of the geochemical and mineralogical characteristics of the Vajont clays will be presented and discussed, along with new laboratory investigations and additional field observations.

Clay samples were collected from both the northern side of the Vajont valley, where the lithostratigraphic sequence is better exposed, and the failure surface of the 1963 Vajont landslide (for the sampling location, see Fig. 3). Field evidence includes the identification of the different geological contexts in which the clay layers occur. Particular attention was paid to the specific stratigraphical situation of the clay interbeds within the limestone sequence involved in the slope failure. Some relevant outcrops were cleaned, pointing out the stratigraphical contacts, and coded, photographed and drawn. The outcrops of clayey materials were accurately prepared before the sampling procedure: the surface debris and the soil cover were always removed, thus avoiding or limiting possible physical (e.g., induration) and/or mineralogical changes caused by

226 weathering processes. The clays were generally found preserved. Additional
227 observations were acquired on the stepped morphology of the basal rupture surface
228 exposed on the slide failure scar. The newly acquired geological data allowed us to
229 reconstruct the two updated lithostratigraphic columns referring to both sides of the
230 Vajont valley (Fig. 4).

231 *3.2. Mineralogy and chemistry*

232 The mineralogy of the sampled clays was investigated in more detail here, specifically
233 as regards the characterisation of illite/smectite (I/S) interstratifications, according to the
234 criteria illustrated in Moore and Reynolds (1997). The degree of ordering between illite
235 and smectite in mixed layers, that is the Reichweite *R*-type, and the illite percentage
236 (%I) in I/S mixed layers was thus determined for each sample. Calcimetric analyses
237 were performed on the sampled clayey materials in order to determine the content of
238 calcium carbonate by using a "De Astis" calcimeter at a temperature of 20°C. The
239 analyses were performed at the Chemical Laboratory of the Department of Physical
240 Sciences, Earth and Environment of the University of Siena (Italy).

241 Trace element geochemical data was determined through X-ray fluorescence
242 analyses that were performed via a WDS sequential Philips PW2400 spectrometer at the
243 Department of Geosciences of the University of Padua (Italy). The analyses were
244 performed on glass bead samples (1:10 ratio with flux Li2B4O7). For the determination
245 of the trace elements, precision is within 3% and detection limits are: 10 ppm for Ba,
246 La, Ce and Nd; 6 ppm for Cr; 5 ppm for V, Ga and Pb; 3 ppm for Co, Ni, Cu, Zn, Rb,
247 Sr, Y, Zr, Nb, Th and U.

248

249 **4. The clays involved in the Vajont landslide**

250 *4.1. Field characterisation*

251 The lithostratigraphical sequence occurring along the final stretch of the Vajont valley
252 includes a complex limestone sequence dating from Middle Jurassic to Upper
253 Cretaceous that is almost entirely exposed on the northern valley side, near the village
254 of Casso. The outcropping geological formations (Fm.) are the following, from the
255 bottom to the top ("Casso sequence" in Fig. 4):

256 - Calcare del Vajont (OOV);
257 - Fonzaso (FOZ);
258 - Ammonitico Rosso Veronese Superiore (ARV_3);
259 - Maiolica (MAI);
260 - Scaglia Variegata Alpina (lower member VAA_1 and upper member VAA_2); and
261 - Scaglia Rossa Friulana (SAA).

262 On the northern slope of Mt. Toc (southern valley side), the lithostratigraphic sequence
263 that was involved in the 1963 Vajont landslide ("Mt. Toc sequence" in Fig. 4) has some
264 differences if compared with the Casso sequence, since it does not include the overlying
265 Scaglia Rossa Friulana Fm., and exhibits variable thicknesses of some geological
266 formations, in particular of ARV_3. A part of the Jurassic–Cretaceous sequence was
267 involved in the formation of the shear zone at the base of the Vajont landslide
268 (Paronuzzi and Bolla, 2012 and 2013), which formed as a result of the prehistoric Mt.
269 Toc rockslide that occurred in the Late Pleistocene–early Holocene period (Paronuzzi
270 and Bolla, 2015a). The geological formations included in the shear zone are, from the
271 bottom to the top: the upper two thirds of FOZ, ARV_3, MAI, and the first 10–15 m of
272 VAA_1 (Fig. 4).

273 The basal failure surface of the slide mainly coincides with the bedding planes of
274 the 5–10 cm-thick cherty limestone layers of the Fonzaso Fm. Borehole data acquired

from drilling of the bedrock performed after the 1963 landslide on the western border of the detachment surface (borehole R7; see Martinis, 1978) shows that the basal failure plane there is located about 25 m above the stratigraphic contact with the underlying OOV. Unfortunately, no borehole data exists for the bedrock stratigraphy on the eastern part of the detachment surface.

The Fonzaso Fm. includes several clay interbeds of variable thicknesses, from 0.5 cm to 6 cm in most cases, but some layers up to about 20 cm-thick occur in the Casso stratigraphic sequence. The clay interbeds are not evenly distributed within the whole 40–45 m-thick Fonzaso Fm. In fact, the lowest 10–15 m stratigraphic beds of FOZ (lower half of the Listato Member, LM) do not include any clay layers (Fig. 4), as visible near the Vajont dam, where the stratigraphic contact between OOV and FOZ is clearly exposed. On the contrary, frequent clay interbeds characterise the upper sequence of the Fonzaso Fm. (30−40 m, that is at the top of the Scisti ad Aptici member, SAM; Fig. 4).

Several 1.0–18.5 cm-thick clay layers were observed in a rock outcrop located on the north valley side, to the west of the village of Casso (Figs. 3, 5a), in correspondence with the stratigraphic contact between FOZ and the overlying ARV_3. This small rock scarp is the same outcrop studied by Hendron and Patton during their field investigations (outcrop 8−1, see Photos 1−3 and Figure 14 in Hendron and Patton, 1985). The 130 cm-thick sequence includes five greyish and yellowish clay layers (VA09-1A−E) interbedded with layers of grey cherty limestone and greenish marly limestone (Fig. 5b). These clay layers extend laterally about 10–15 m. The clay interbed coded as VA09-1B is the thickest layer ever surveyed in the Vajont valley. This outcrop is particularly important since it provides field evidence that multiple clay layers are concentrated within certain parts of the limestone sequence. As shown in Fig. 5, five 1

300 to 18.5 cm-thick clay interbeds occur in a 1.3 m-thick sequence of cherty limestone
301 layers.

302 The basal rupture surface exposed on the failure scar of the 1963 Vajont landslide
303 (western and eastern limestone slabs in Fig. 3) has a marked stepped morphology
304 (Wolter et al., 2014; Paronuzzi and Bolla, 2015a). Two orders of rock steps can be
305 identified, on the basis of their strike compared with the dip direction of the
306 stratification joints, which is close to the main sliding direction (Fig. 6). Lateral steps
307 occur in directions that are sub-parallel or oblique to the dip direction of the rock strata,
308 whereas transverse steps occur sub-orthogonally to the latter (Fig. 6a, b). In most cases,
309 the lateral steps have a height varying between 1 m and 5 m (Fig. 6c), and mainly
310 coincide with large tectonic fractures or pre-existing macro-joints (Paronuzzi and Bolla,
311 2015a). On the other hand, as demonstrated in Fig. 6d, the transverse steps are smaller
312 and exploit newly formed fractures related to the slope progressive failure (i.e., gravity-
313 induced joints; Paronuzzi and Bolla, 2015b) within a single 5 to 10 cm-thick limestone
314 layer or a series of beds between 0.5 and 1 m-thick.

315 These steps form rock scarps that expose different parts of the bedrock beneath
316 the basal sliding surface. When considering all these steps, a total thickness of about
317 15–20 m of the FOZ sequence is exposed on the large failure scar of the slide.
318 Interestingly, clay interbeds within the in-situ limestone sequence outcropping on the
319 detachment surface are very rare, since only one clay layer was therein identified during
320 the field surveys (VA15-166 in Figs. 3 and 6b). This clay layer is located very close to
321 the clay interbed exhumed by Hendron and Patton (1985) and shown in Fig. 2.

322 Remnants, up to 10–12 m-thick, of the primary shear zone are visible in several
323 outcrops on the western and eastern basal shear surfaces (Fig. 3). The shear zone
324 material includes limestone angular gravel that underlies or completely wraps large

blocks of strongly fractured and folded stratified rock masses (Paronuzzi and Bolla, 2012). Clayey materials were identified in different geological contexts related to the basal shear zone of the Vajont slide (Fig. 7): clay layers occur as lenses or interbeds (i) at the basal failure surface (Fig. 7a, b), (ii) within the displaced stratified rock masses (Fig. 7c, d), or (iii) they are mixed with the limestone angular gravel (Fig. 7e, f).

Clay lenses occurring at the basal sliding surface are commonly characterised by a thickness of 3–7 cm. Differently, the clay layers included in the stratified rock masses are isolated 0.5 to 2 cm-thick lenses or interbeds of grey, greenish, and yellowish clay. However, most of the clay layers identified on the field are included in the limestone angular fragments originated by the disintegration of the rock strata. In some circumstances, 1 to 4 cm-thick clay layers of variable colours appear as spread, contorted and discontinuous lenses. In many cases, multiple and overlying clay lenses are concentrated in 1 to 2 m-thick debris strips. Field observations also ascertained that, in any case, the clay lenses have continuity lower than 10–15 m.

4.2. Mineralogical and geochemical characterisation

XRPD analyses ~~on < 2 μm fraction that were~~ reported by Bolla et al. (2020) showed that the clay layers consisted mainly of clay minerals, calcite and quartz (Table 2). Semi-quantitative estimation of clay and non-clay minerals was performed on bulk samples by measuring peak areas in the diffractograms of each phase, as described in Bolla et al. (2020). When referring to clay minerals, the detailed analysis of air-dried, heated and ethylene glycolated oriented mounts performed on the < 2 μm fraction showed the almost exclusively occurrence of illite/smectite (I/S) mixed layers in all the investigated sediments. Other minerals occurring in some samples as traces only were: K-feldspar, kaolinite, illite and probably chlorite (Table 2).

However, a very complex admixture of I/S with different illite contents and degrees of ordering was outlined in different samples. In particular, samples VA07-3A, VA07-3B, VA07-8, VA09-1A and VA09-1B showed a prevalence of I/S mixed layers with *R*0 stacking order (50–60% illite layers) and subordinate I/S of the *R*1 type with a variable illite content (Table 2). The remaining samples were characterised by a prevalence of the *R*1 stacking order with a variable illite content. In detail, samples VA07-5A and VA07-11A were characterised by both *R*1 and *R*0 stacking orders with I% ~ 60–70% and I% ~ 50%, respectively; whereas samples VA07-13C and VA07-14 showed almost exclusively I/S *R*1 with about 70–80% of illite (Table 2).

According to the semi-quantitative estimation of the mineral content for each investigated sample, two well-defined groups of samples were distinguished (Bolla et al., 2020; Table 2). Samples VA07-3A, VA09-1A, VA09-1B, VA07-11A (Fig. 8a, b), VA07-13C and VA07-14 showed a large amount of clay minerals, from 79% up to 96%; whereas samples VA07-3B (Fig. 8c, d), VA07-8 and VA07-5A were characterised by a higher content of calcite, from 34% up to 64% (Fig. 9a). Amounts of quartz did not exceed 6% in the investigated samples. Calcite contents determined through the semi-quantitative estimation were always slightly lower than corresponding $CaCO_3$ percentages that were obtained by means of the calcimetric analyses (Table 2). However, the average difference between the two data sets was 4.8%, which represents quite good agreement.

Major oxide geochemical data (see Table 1 in Bolla et al., 2020) correlates well with the amounts of clay minerals and calcite occurring within the analysed samples. In fact, the contents of SiO_2, Al_2O_3 and K_2O were, on average, higher for clay-rich samples and lower for calcite-rich samples. On the contrary, loss on ignition (LOI) and the content of CaO were higher for calcite-rich samples and lower for clay-rich samples.

374 This means that SiO_2, Al_2O_3 and K_2O were strictly correlated with the I/S mixed layers,
375 as expected, whereas CaO was mainly associated with calcite.
376 Table 3 shows the trace element geochemical data of the Vajont clays. The
377 average content of Zr, Zn, Ba and Ni was higher than 100 ppm, Cu, Rb and Sr were in
378 the range 50–100 ppm, V, Co, Ga, Y, La, Ce, Nd, Pb and Th were within 10 and 50
379 ppm. Chromium, Nb and U were below 10 ppm. The content of some trace elements
380 was found to be strongly dependent on the mineralogical composition of the analysed
381 samples, since these elements were strictly associated with clay minerals rather than
382 other minerals (or colloids) occurring in the sampled soils. For example, V, Sr, Y, La,
383 and Nd were at their highest for calcite-rich sample VA07-5A and at their lowest for
384 clay-rich sample VA07-14; whereas the opposite (i.e., lowest vs. highest) was observed
385 for trace elements Ga and Zr occurring in the same samples (Table 3).
386
387 **5. Genesis and provenance of the Vajont clays**

388 *5.1. The Vajont K-bentonites*

389 All the Vajont clay samples showed a very similar mineralogical composition and
390 geochemical fingerprint. The dominant clay minerals were I/S mixed layers with a 85–
391 50% content of illite layers, thus predominating over smectite (Table 2). This is
392 consistent with the geochemical data that emphasised a significant percentage of K_2O
393 (1.17–5.77%) in the sampled clays (see Table 1 in Bolla et al., 2020). Smectite-rich
394 clays were identified in many rock mass sequences of various geological ages as a
395 consequence of detailed lithostratigraphic analyses that allowed for the recognition of
396 very thin layers of clays (mm- or cm-thick), often with high-plasticity properties,
397 interbedded within various rock strata sequences (Huff, 2016 and references therein).
398 Those particular clays were interpreted as deposits of volcanoclastic materials (tephra),

399 sometimes altered by hydrothermal processes or by diagenesis, representing key
400 stratigraphic levels that are very useful for chronological correlations of different
401 lithostratigraphic sequences (tephrochronology). Smectite-rich clays were also indicated
402 as bentonites or K-bentonites (Huff, 2016), depending on the percentage of potassium
403 that is accounted for by illite. Mineralogical and geochemical data shown in the present
404 study indicates that the Vajont clays included in the Fonzaso Fm. can be described as K-
405 bentonites, considering the high percentage of illite that was identified as I/S mixed
406 layers in the sampled clays.
407 The bentonites of the Vajont valley can be interpreted as distinct tephra levels, i.e.
408 repeated volcanoclastic events causing sedimentary inputs of volcanic ashes that
409 interrupted the "normal" calcareous sedimentation within this small Jurassic basin at the
410 easternmost boundary of the Belluno Trough. Stratigraphic field evidence highlights the
411 occurrence of several mm- or cm-thick clay layers alternated with 5–10 cm-thick platy
412 cherty limestone beds, often occurring as 3–5 distinct layers within a 1–2 m-thick rock
413 sequence (Fig. 5). This evidence demonstrates that explosive volcanic events occurred
414 with a certain frequency during the Upper Jurassic, originating multiple tephra levels.
415 K-bentonites of the Fonzaso Fm. exhibited rather constant geochemical and
416 mineralogical characteristics (dominance of I/S mixed layers), for both the tephra
417 involved in the basal rupture of the Vajont landslide and those sampled within the in-
418 situ lithostratigraphic sequence outcropping near the village of Casso on northern side
419 of the Vajont valley. This fact emphasises a strong mineralogical similarity between the
420 K-bentonites sampled within the two sedimentary sequences, suggesting the same
421 volcanic source and also a comparable geological age: the possible maximum difference
422 in age between the two tephra sequences is in the order of 0.1–0.3 to 1–3 Ma. When
423 considering the whole lithostratigraphic sequence (Fig. 4), the tephra levels of the

Fonzaso Fm., in absence of specific biostratigraphic studies or absolute dating, could tentatively be attributed to the late Oxfordian–upper Tithonian, and an age within the time span 158–145 Ma seems to be the most probable (Luca Martire, personal communication). This is the first recognition of bentonitic layers within the Upper Jurassic Fonzaso Fm., that is a typical cherty limestone sequence characterising the larger Belluno Basin located westward to the Vajont valley.

5.2. Genesis of the I/S mixed layer clays

I/S mixed layers with different percentages of illite commonly occur in ancient bentonites of various ages (Huff, 2016 and references therein). According to a widespread literature (Bethke et al., 1986; Cuadros and Altaner, 1998; Inoue et al., 2005), these minerals are intermediate members of the progressive reaction of smectite-to-illite conversion known as smectite "illitization", which occurs as the result of diagenetic or hydrothermal processes. Temperature is considered the main factor controlling this transition (Merriman and Peacor, 1999; Árkai, 2002; Merriman, 2005; and reference therein), although other variables such as time (Pytte and Reynolds, 1989), availability of K (e.g. Huang et al., 1993; Weibel, 1999) and fluid circulation (Eslinger and Pevear, 1988) may also significantly influence the process. According to a diagenetic origin, the illite content and ordering of illite/smectite, from random I/S (*R*0 with S > 50%; Moore and Reynolds, 1997) up to ordered I/S (*R*1 and *R*3 with I > 50%; Moore and Reynolds, 1997), are commonly interpreted as indicators of degree of burial diagenesis.

In contrast to previous descriptions, Lanson et al. (2009) described a two-stage process of smectite illitization. The early stage is characterised by the coexistence of discrete smectite and randomly, illite-rich (I > 50%) I/S interstratified. With increasing burial depth, they found an increase in the relative proportions of I/S, essentially at the

449 expense of discrete smectite, with a slightly more illitic composition in the I/S mixed
450 layers. In the second stage of smectite illitization, two illite-containing mixed layers
451 were observed (Lanson et al., 2009). According to Fang et al. (2017), the smectite
452 illitization of volcanoclastic bentonites may also be the result of microbial activities that
453 induce dissolution and precipitation processes.

454 If we consider the widely accepted diagenetic theory as the main process causing
455 the smectite illitization of the Vajont clay interbeds, a low diagenetic maturity is
456 generally suggested in most of the investigated samples (VA07-3A, VA07-3B, VA07-8,
457 VA09-1A and VA09-1B) owing to the occurrence of appreciable amounts of I/S *R*0
458 ordering type and an illite content of around 50%. The concurrent presence of I/S *R*1
459 with higher illite percentages in the same samples suggests that these minerals may have
460 been inherited from the neighbouring area at the time of deposition.

461 The occurrence of a prevailing or exclusive *R*1 ordering type with high illite
462 contents in the other samples (VA07-5A, VA07-11A, VA07-13C and VA07-14) may
463 suggest a higher diagenetic maturity, but further evidence is necessary to validate this
464 hypothesis. Interestingly, a prevailing I/S *R*1 type occurred in clay samples that were
465 acquired from the eastern limestone slabs outcropping on the detachment surface of the
466 slide, whereas the I/S *R*0 mixed layer minerals were mainly associated with clay layers
467 sampled from the western limestone slabs and from the in-situ lithostratigraphic
468 sequence outcropping near the village of Casso (Figs. 3 and 4 and Table 2). However, a
469 more detailed correlation between the different lithostratigraphic sequences outcropping
470 on the failure scar needs a further investigation, for instance by means of
471 biostratigraphic data.

472 When considering the genesis of the I/S mixed layers of the investigated
473 sediments, it is also necessary to examine the possible origin of the primary smectite

474 minerals occurring in the tephra levels that were further included in the Vajont clay
475 interbeds. The formation of smectite minerals is very often related to volcanic rocks,
476 both mafic and felsic rocks, and volcanoclastic sediments. However, the suggested
477 formation process for smectites in volcanoclastic deposits can be very variable and
478 includes: (i) the hydrothermal origin caused by the alteration of volcanic glass particles
479 (Fiore, 1993; Mirabella et al., 2005) or by the precipitation from fluids that are mixtures
480 of magmatic and local meteoric water located within volcanic vents (Mizota and Faure,
481 1998); (ii) the deuteric alteration, i.e. a low-temperature magmatic alteration related to
482 the solidification of a melt (Spinola et al., 2017); and (iii) the weathering of volcanic
483 ashes during the early stages of diagenesis at the sediment/seawater interface (Pellenard
484 et al., 2013).

485 The latter formation process is generally assumed for most of the bentonite
486 deposits in which the middle alkalinity of marine environment favoured the alteration of
487 volcanic ash into smectite (Velde, 1995; Murray, 2006). The first two cases
488 (hydrothermal and deuteric alterations) presuppose a primary volcanogenic origin. In
489 fact, smectite-rich volcanoclastic deposits were actually ascertained in the surrounding
490 area of modern day volcanoes (Fiore, 1993; Mizota and Faure, 1998; Mirabella et al.,
491 2005), confirming the possible formation of smectite directly within active volcanic
492 edifices. In certain cases, the origin of smectite-rich clays is attributed to the alteration
493 of volcanoclastic rocks and lavas emplaced under marine conditions, that is caused by
494 devitrification of the original volcanic glass or by hydrothermal processes (Christidis
495 and Dunham, 1993).

496 When considering the various proposed interpretations of smectite-rich ashes
497 emitted in the atmosphere by present volcanoes, it is probable that the original
498 volcanoclastic powders contained a significant amount of smectite particles mixed with

499 volcanic glass and quartz, even if a further alteration of the tephra at the
500 sediment/seawater interface, caused by a cation exchange and Mg enrichment
501 (Compton, 1991), cannot be excluded. This may possibly account for admixtures of
502 mixed layers of different nature in the investigated samples.

503 The mineralogical composition of the bentonites sampled within the Fonzaso Fm.
504 emphasises that the original volcanic ashes were mixed with other intra-basin marine
505 sediments made up of calcite crystals. In fact, the sampled Vajont clays always
506 contained a certain amount of calcite that ranges from low (5–19%) to moderate (23–
507 43%) and high percentages (66%), as shown by the calcimetric analyses (Table 2). The
508 variable mixture of volcanoclastic material with calcareous fine-grained autochthonous
509 sediment originated different mineralogical assemblages, where volcanic ashes
510 predominate (Group 1) or where marine calcite-rich sediments prevail (Group 2), even
511 if an intermediate situation can also occur. These two main mineralogical assemblages
512 can clearly be recognised on examining the geochemical and mineralogical features of
513 the analysed clays (Fig. 9b). Group 1 shows higher percentages of clay minerals (79–
514 96%) associated with considerable amounts of K_2O (2.60–5.77%, in most cases). On the
515 contrary, Group 2 shows lower percentages of interstratified illite/smectite minerals
516 (36–60%), with the lowest values of K_2O (1.17–2.30%).

517 It is interesting to note that the variable mixture of tephra and marine sediments
518 characterises the single volcanoclastic sedimentation event, so that thin, immediately
519 overlying bentonites can reveal very different relative percentages between volcanic-
520 derived materials and marine calcite-rich sediments. This evidence has been recognised
521 both on the large failure surface of the Vajont landslide (outcrop VA07-3: samples
522 VA07-3A and VA07-3B) and within the lithostratigraphic sequence of Casso (outcrop

523 VA09-1: samples VA09-1A, VA09-1B and VA09-1E), where near-pure volcanoclastic
524 levels are alternated with tephra strongly mixed with marine calcite-rich sediments.

525 *5.3. Provenance*

526 During the Jurassic, there were massive outpourings of basaltic igneous rocks, mass
527 extinctions, significant variations in climate, sea level, atmospheric CO_2 and anoxic
528 episodes (Hesselbo et al., 2002, 2007). Epicontinental seas occupied large parts of
529 western and central Europe by the end of the Early Jurassic. Infilling sediments were
530 predominantly sourced from the east due to the uplift occurring in the East European
531 Platform and the Bohemian massif. According to Ziegler (1990), the rift systems that
532 initiated during the Early Triassic remained active during the Early Jurassic. During the
533 Jurassic period, the southern Tethyan continental margin was affected by extensive
534 tectonics related to syn-rift and early post-rift phases while, in the Alpine domain,
535 rifting became increasingly important in the South Alpine and Austroalpine realms even
536 if rift-related volcanism was at a very low level (Ziegler, 1990).

537 Latin and Waters (1992) and Quirie et al. (2019) reported that moderately to
538 highly alkaline volcanic activity accompanied the formation of the North Sea rift dome
539 in the late Bajocian–Bathonian times. Studies by Berra et al. (2009), Basilone et al.
540 (2010) and others confirmed tectonic control of the Triassic and Jurassic pelagic
541 sediments of the Southern Alps, Apennines and western Sicily. There, submarine to
542 subaerial episodes are reported for the Bajocian–Bathonian (Basilone et al., 2010) while
543 Upper Jurassic is represented by porfiric basalts rich in pyroxenes and plagioclases with
544 rare olivine. Moreover, the Alpine Tethys ophiolitic system (Ligurides / Piedmont /
545 Valais) occurred in late Middle Jurassic time (ca. 185–155 Ma; Lenaz et al., 2019 and
546 references therein).

I/S mixed layer minerals, Ca-smectite, quartz and calcite in different amounts made up the studied materials. Traces of chlorite and kaolinite were present. What could the provenance of these clayey materials be? According to Wang et al. (2013), felsic sources are characterised by low Cr/V and Co/Th ratios and high Y/Ni and La/Sc ratios, while an ophiolitic source would have high amount of Cr and Sc. In the studied samples, the low Cr content and the Sc content below the detection limit allow us to exclude a mafic source (and consequently the ophiolitic products), pointing to, at least, an intermediate source. This fact is also confirmed by the high amount of Zr. Interestingly, Zhang et al. (2013) suggested that Zn, Ba and Pb could be related to some hydrothermal processes, and Zn and Ba were among the highest trace elements recorded in our samples. Moreover, the same authors recognised the so-called feldspar- and mica-trend relating Rb and K_2O that for our samples suggest a possible derivation from the weathering of micas (Fig. 10).

In order to decipher the possible geological setting for different materials, Bhatia and Crook (1986) proposed the ternary diagram Th-Co-Zr/10. In this diagram, some of our samples fall into the Continental Island Arc field while some others are close to the Active Continental Margin presenting a small Th-excess (Fig. 11a). This could be due to the fact that smectite acts as host for Th (Kelepertsis, 1981; Hein et al., 1982). Low Nb content could be related to a subduction environment (Meijers et al., 2010). Finally, the Zr/Ti vs. Nb/Y diagram (Winchester and Floyd, 1977) suggests a dacite/rhyodacite to rhyolite source, apart from one sample showing a possible trachytic provenance (Fig. 11b).

Geochemical analyses of clayey deposits of Jurassic age are rare. Pellenard et al. (2003) analysed the bentonite deposits of the Oxfordian in the Paris basin and the Callovian–Oxfordian deposits of the Hautes-Alpes department (SE France).

572 Biostratigraphical and geochemical data suggests that the thick bentonite in the Paris
573 Basin correlates with the thickest bentonite in the Subalpine Basin, located 400 km to
574 the south. Those bentonites were characterised by high concentrations of Hf, Nb, Pb,
575 Ta, Th, Ti, U, Y, Zr and low concentrations of Cr, Cs and Rb. Those horizons indicate
576 that significant explosive volcanic events occurred during the Middle Oxfordian. The
577 chemistry of those bentonites corresponds to a trachyandesitic source from a within-
578 plate alkaline series that was probably related to the North Atlantic rifting.

579 Even if the age is similar, the chemistry of our samples suggests a different source
580 related to a more felsic volcanism. Some smectite-rich clays or bentonites were already
581 recognised in some Upper Jurassic sedimentary sequences of the Italian Alps (Veneto
582 and Trentino regions, northern Italy). In the Ammonitico Rosso Veronese Superiore
583 (ARV_3), Bernoulli and Peters (1970) found thin intercalations of bentonitic clays that
584 they related to a rhyolitic with a tendency to trachytic source. Considering that the
585 material was very fine grained they supposed a distant source (Bernoulli and Peters,
586 1970).

587 Eight volcanic ash layers (bentonites) interbedded with marine limestones and
588 cherts were identified in the ARV Formation and were dated to 156.1 ± 0.89 Ma
589 through a ^{40}Ar–^{39}Ar radiometric dating (Pellenard et al., 2013), that is consistent with a
590 late Oxfordian–early Kimmeridgian age. These bentonites were interpreted as
591 volcanoclastic layers linked to large explosive events caused by the subduction-related
592 volcanism from the Vardar Ocean back-arc. The analysed bentonites include “pure
593 smectite horizons” and “occasional volcanic crystals (e.g. sanidine, quartz, biotite)”, but
594 no specific mineralogical analyses of clay minerals were reported (Pellenard et al.,
595 2013). The geochemical signature of the bentonitic levels recognised in the ARV

596 Formation indicates that the primary ash layers derived from an evolved calc-alkaline
597 magma.

598 Far to the East, the earlier Mesozoic evolution was dominated by opening and
599 closure of Tethyan oceans between Gondwana and Laurasia with their consumption, at
600 least in part, accommodated along the southern Eurasian margin. Crimea (Ukraine)
601 represents the northernmost region of southeastern Europe that exposes a record of a
602 pre-Cretaceous Tethyan active margin. There, middle Jurassic (~172–158 Ma) and
603 uppermost Jurassic to lowermost Cretaceous (~151–142 Ma) terranes with a
604 subduction-related geochemical signature outcrop (Meijers et al., 2010). Within the
605 Middle Jurassic products, dacitic and ryolitic magmas are present.

606 For comparison purposes, the spidergrams of trace elements for different
607 materials with a possible common provenance are represented in Fig. 12: (i) the
608 bentonites from Vajont (this study); (ii) the bentonites from the Trento Plateau
609 (Pellenard et al., 2013); (iii) the pyroclastics deposits from the Vardar subduction zone
610 (Bonev and Stampfli, 2008); and (iv) the intermediate to felsic rocks from the Crimea
611 subduction zone (Meijers et al., 2010). As can be seen from the spidergrams, the
612 patterns are rather similar, apart from the trend of the Vardar ones that is almost flat in
613 the part from Nb to Y. Geochemical data of the Vajont bentonites shows a good
614 correspondence with the geochemical fingerprint of the bentonites intercalated in the
615 Ammonitico Rosso Veronese and with the Vardar volcanoclastics, thus a common
616 source and provenance can be hypothesised. However, the Crimea subduction zone
617 could be another possible source of the clay layers occurring in the Vajont sequence.
618

619 **6. Geotechnical properties vs. mineralogical composition**

620 Grain-size distribution analyses performed on the Vajont clays and reported by Bolla et
621 al. (2020) showed that the investigated clay layers can be described as silty clays and
622 clayey sandy silts, according to the EN ISO 14688 identification and classification of
623 soil. The plasticity properties of these fine soils are rather variable, with the liquid limit
624 (LL) ranging from 38% to 89% and the plasticity index (PI) varying from 21% and 59%
625 (Fig. 13). The plasticity chart of Fig. 13 also correlates the plasticity properties of the
626 Vajont K-bentonites with both their mineralogical composition and the different
627 geological contexts referred to the landslide in which the clay layers occur. When
628 considering the latter issue, the clay lenses localised at the basal contact with the shear
629 zone have an intermediate-to-high plasticity. The tephra levels found in the upper part
630 of the in-situ sequence of the Fonzaso Fm. and the clay layers admixed with the
631 limestone angular gravel have an intermediate plasticity (Fig. 13), even if some samples
632 fall outside the field included between the A-line (Casagrande, 1948) and the U-line
633 (ASTM, 1993). Finally, clay interbeds included in the displaced rock masses were
634 found to have highly variable plasticity. However, on the whole, no clear or
635 unambiguous relationship emerges between the plasticity properties and the geological
636 contexts of the sampled soils.

637 Differently, the plasticity properties of the Vajont clays are clearly influenced by
638 their mineralogical composition. In fact, calcite-rich samples are characterised by an
639 intermediate-to-low plasticity, whereas clay-rich samples have an intermediate-to-high
640 plasticity (Fig. 13). In more detail, the clay mineral content of the fine-grained soils has
641 influence on their liquid limit, even if a low correlation coefficient characterises the
642 exponential relationship (Fig. 14a). Indeed, clay-rich samples (CM > 79%) are
643 characterised by values of LL ranging from 52% to 89%; whereas samples with a lower
644 content of clay minerals (CM < 60%) have LL values from 38% up to 62%. When

645 analysing the different geological contexts related to the landslide, clay layers
646 characterised by intermediate values of the liquid limit (50% < LL < 70%) mainly occur
647 within the disintegrated rock mass of the basal shear zone of the slide. Clay beds with
648 the highest values of LL (71–89%) occur in correspondence of the basal sliding surface
649 or in the in-situ limestone sequence at the top of the Fonzaso Fm (Fig. 14a).

650 Residual shear strength properties of the Vajont K-bentonites were reported by
651 Bolla et al. (2020). The ring shear tests, which were performed at 200–600 kPa effective
652 normal stress, revealed a strong influence of the mineralogical composition on the
653 residual shear resistance. In fact, as visible in the diagram of Fig. 14b, the lowest values
654 of the residual angle of internal friction (7–15°) were obtained for the clay samples with
655 the largest content of clay minerals (CM > 79%), whereas clay layers with a higher
656 content of calcite and quartz were characterised by greater values of the residual friction
657 angle (20–27°). This close relationship is also emphasised by the high correlation
658 coefficient of the exponential trend (Fig. 14b). However, it must also be noted that there
659 is no correlation between the low-shear strength bentonites and the specific geological
660 context in which the clay lenses occur. Indeed, clay-rich soils with low values of the
661 residual angle of internal friction indifferently occur in the in-situ limestone sequence,
662 at the basal failure surface of the slide, within the displaced rock masses and within the
663 disintegrated rock mass of the basal shear zone (Fig. 14b). This evidence has to be kept
664 in mind when analysing the influence exerted by the shear strength properties of the
665 clay interbeds on the specific lithostratigraphic position of the basal failure surface of
666 the Vajont slide.

667 On the whole, the geotechnical properties of the Vajont clays are strongly
668 dependant on the content of clay minerals within the tephra layers, whereas the specific
669 structure of the I/S mixed layers had no influence on the plasticity and residual shear

strength properties of the clays. In fact, the recognised *R*0 and *R*1 Reichweite ordering types and the related illite percentages over smectite (Table 2) characterise both low-plastic and high-plastic clays as well as both low-strength and high-strength clays (Figs. 13 and 14).

7. Geomechanical implications of the tephra layers

The presence of weak illite/smectite mixed layer clays within the Jurassic limestone sequence located at the base of the giant 1963 Vajont landslide has a notable scientific meaning as these bentonitic layers affected in a decisive manner the onset and evolution of the large instability processes on the northern slope of Mt. Toc. During the first studies, the occurrence of these low-strength clay layers was strongly debated due to the limited field evidence for the presence of plastic clayey materials, but also because the knowledge about rock masses with intercalated soft clay beds was very poor at that time (1950–1960). The geomechanical implications related to these thin volcanoclastic levels are key for the comprehensive understanding of the evolution of the distinct instability processes that involved the northern slope of Mt. Toc during a time interval of about 18,000–15,000 years, i.e. after the last glacial maximum (LGM).

In fact, the northern slope of Mt. Toc experienced multiple landslide events that can be summarised in (Paronuzzi and Bolla, 2015a): (1) the prehistoric slope failure that occurred in the late Pleistocene–early Holocene and was characterised by a multi-stage rupture including two major primary or first-time failures; and (2) the 9 October 1963 landslide reactivation that remobilised as a single block the previously failed landslide bodies that rested on a basal shear zone of highly variable thickness (10–50 m). Both major landslide events were favoured by three decisive predisposing geological factors: (i) the general dip-slope attitude of bedding planes on the northern slope of Mt. Toc; (ii)

695 the presence of a number of continuous intersecting faults that delimited potentially
696 unstable blocks with a large volume and a near-rectangular shape; and (iii) the
697 occurrence of the high-plastic and low-strength I/S mixed layer clay interbeds within the
698 cherty limestone sequence in the upper half of the Jurassic Fonzaso Fm. The
699 unfavourable combination of these three geological conditions was decisive to cause the
700 first prehistoric slope failures as well as the catastrophic slide that occurred on 9
701 October 1963. However, due to the very complex geomorphological evolution of the
702 slope, the geomechanical influence of the low-strength bentonitic layers on the slope
703 instability was different, and it can only be appreciated distinguishing the primary
704 failures from the subsequent remobilisation, when the basal shear zone was already
705 created.

706 The ancient prehistoric Mt. Toc rockslide involved two 100–150 Mm^3-size
707 blocks, i.e., the “Pian del Toc” and “Pian della Pozza” blocks, which collapsed in a
708 consecutive manner originating a partial superimposition of the latter on the back of the
709 former. The time interval that separated these two first-time slope failures is unknown,
710 but their geological similarities seem to indicate a relative short time interval, and a very
711 rapid retrogressive mechanism can be hypothesised (Paronuzzi and Bolla, 2015a). The
712 recently published (Masè et al., 2004) photographic documentation acquired during the
713 geological survey carried out by Rossi and Semenza immediately after the 1963
714 landslide, which was favoured by the washing effect caused by the huge waves that
715 impacted the surface of the failed mass, emphasised the presence of the distinct blocks
716 mobilised by the two main prehistoric slope failures. Field evidence proved that these
717 two blocks were affected by strong gravity-induced rock mass damage related to both
718 pre-collapse (quasi-static) and dynamic (run-out) deformation stages (Paronuzzi and
719 Bolla, 2015a).

When relating to the ancient slope failures, the role of the volcanoclastic interbeds was conclusive to reduce the available shear strength within the upper sequence of the Fonzaso Fm., thus contributing in the onset of the large slope instability processes. Indeed, due to the very low shear strength of the intercalated bentonitic layers, the initial failure mechanism was strongly controlled by the incipient shear displacements along these weak clay layers. It must now be remarked that, as proved by field evidence, the clay interbeds were 0.5–6.0 cm-thick, in most cases, and had a continuity lower than 10–15 m. When considering the large extent of the bedding planes of the cherty limestone sequence, along with their undulations and sin-sedimentary folding possibly related to Jurassic slumping events, the low thickness and continuity of the clay interbeds caused the occurrence of rock-to-rock contacts along the bedding planes, which represent rigid constraints within the multi-layered sequence.

As a result, relative shear displacements occurring within the bentonitic layers or at the clay–limestone boundary induced localised stress concentrations at the rock-to-rock stiff contacts that caused fracturing initiation and propagation at the expense of the limestone beds. The increasing development over time of this characteristic failure mechanism provoked the progressive formation of an incipient shear zone at the base of the unstable slope, with strong rock mass fracturing and/or limestone crushing. Since the volcanoclastic interbeds are concentrated within certain parts of the upper half of the Fonzaso Fm., the critical zone subjected to relative shear slips was not related to a single specific weak clay layer, but rather to a certain stratigraphical sequence including multiple, overlying thin soft clay interbeds. As a consequence, the formation process of the basal shear zone involved a rock mass of considerable depth, reaching the notable thickness of at least 25–30 m.

744 The multiple I/S mixed layer clays also caused the formation of the typical
745 stepped geometry of the basal failure surface of the Vajont landslide, still visible today
746 on the large failure surface. The multiplicity of weak clay interbeds at the base of the
747 Vajont landslide is often not appreciated, and many geotechnical researchers consider
748 the slope failure as driven by the presence of a single basal low-strength clay layer. On
749 the contrary, the widespread occurrence of thin volcanoclastic clay lenses within the
750 upper sequence of the Fonzaso Fm., which were not limited to a single sedimentary
751 event, was decisive to generate a basal shear zone having a considerable and unexpected
752 thickness. At the same time, from a geomechanical point of view, this peculiarity is a
753 distinctive feature of the Vajont landslide and should be considered when simulating the
754 progressive formation and evolution of the basal shear zone caused by the prehistoric
755 slope failures.

756 After the occurrence of the prehistoric slope failures, the morphology of the
757 northern slope of Mt. Toc changed substantially, since the two major failed rock blocks
758 stopped at the bottom of the Vajont valley, obstructing the ancient river flow. The 400–
759 500 m-long propagation of the Pian del Toc and Pian della Pozza blocks caused the
760 disruption of the rock mass at the base of the slide, thus developing a mature shear zone
761 made up of abundant limestone angular gravel, sheared-off rock masses and spread clay
762 lenses. As a result, the failed blocks rested on the underlying thick shear zone
763 characterised by newly formed gravelly-type debris and isolated clay lenses at residual
764 shear strength. This new geological configuration of the slope was completely unknown
765 to the designers of the Vajont dam when the big hydraulic engineering project started
766 and the works officially began on 6 January 1957.

767 The occurrence of a prehistoric landslide was only suspected in Summer 1960,
768 after the first detailed geological survey of the southern bank of the reservoir (Giudici

769 and Semenza, 1960) and when the precursory signs of slope instability have already
770 been revealed (March 1960). However, the occurrence of an ancient large prehistoric
771 landslide lying on the northern slope of Mt. Toc was strongly confuted by other
772 technicians, both geotechnical engineers and geologists, that were consulted at that time
773 to interpret and to manage the incoming large slope instability, which was dramatically
774 emphasised by the huge threatening fissure, the well known "M-shaped" crack,
775 suddenly occurred in late October–early November 1960.

776 The catastrophic collapse of 9 October 1963 was a classic example of
777 remobilisation of an ancient landslide, which was induced by three repeated filling–
778 drawdown cycles of the reservoir that were performed, with some interruptions, since 2
779 February 1960, and was followed by the unforeseen en-block sliding motion. During
780 this man-induced landslide remobilisation, the geomechanical role of volcanoclastic
781 interbeds was different, when compared with the influence played by the clays to
782 activate the first-time slope failures related to the prehistoric instability. As a result of
783 the rock mass comminution at the base of the slide, the clay layers formed very irregular
784 and discontinuous lenses with moderate planar extension, and the shear zone material
785 was dominated by the highly permeable limestone angular gravel. This means that the
786 clay layers represented isolated thin lenses without any effect on the overall hydraulic
787 conductivity of the shear zone material. The groundwater inflow induced by the
788 reservoir level changes was exclusively influenced by the high permeability of the
789 gravelly soils, without any actual sealing effect provided by the isolated clay lenses.

790 During the final slope instability, most clay lenses were characterised by a
791 residual shear strength caused by the considerable displacements that had previously
792 cumulated as a consequence of the prehistoric failures. Obviously, the low-resistance
793 I/S clay lenses contributed in reducing the available shear strength along the future

794 failure surface of the 1963 slide, which partially formed within the shear zone material
795 and partially reworked the dip-slope bedding planes of the Fonzaso Fm. (Fig. 3).
796 However, the decisive landslide trigger was the variation in the pore water pressures
797 along the failure surface, in particular the decrease in the effective stresses caused by
798 the groundwater inflow related to the reservoir impoundments. This means that the role
799 of the volcanoclastic clays was secondary or subordinate in the occurrence of the
800 catastrophic 1963 landslide remobilisation, whereas in this circumstance, the presence
801 of the highly permeable limestone angular gravel of the shear zone was decisive.
802
803 **8. Conclusions**
804 The presence of soft clay layers intercalated within the Fonzaso Fm. dated to the Upper
805 Jurassic was an unexpected geological feature and, for this reason, was strongly debated
806 by the first researchers dealing with the Vajont landslide, especially by Leopold Müller,
807 the major geotechnical engineer involved in the construction of the hydroelectric power
808 plant at Vajont. This is not surprising, especially if we consider the state of the
809 geological and geotechnical knowledge dating back to 1960 or immediately after. The
810 presence of a prehistoric rockslide lying on the northern slope of Mt. Toc was and, for
811 some researchers, still is a contended issue. Although the 1963 Vajont landslide has
812 been analysed from different scientific points of view, previous studies never examined
813 the problem of the particular mineralogical nature of the clays involved in the slope
814 rupture and, in particular, their geological origin and provenance.
815 The mineralogical investigations of the clay interbeds occurring within the
816 Fonzaso Fm. and outcropping in the Vajont valley showed the occurrence of complex
817 assemblages of illite/smectite (I/S) mixed layers admixed with variable amounts of
818 calcite and quartz (Bolla et al., 2020). On the whole, the investigated clay samples were

819 characterised by highly variable contents of clay minerals (CM = 36–96%), calcite (Cal
820 = 4–64%) and quartz (Qtz = 0–6%). However, only *R*0 and *R*1 Reichweite ordering
821 types were recognised, with an illite content ranging from 50% up to 85%, suggesting a
822 low-to-medium degree of smectite-to-illite diagenetic transformation. The abundance of
823 illite in the mixed-layers assemblage is confirmed by the high percentage of potassium
824 as revealed by the geochemical analyses of the sampled clays.
825 On the basis of the study carried out, the clays interbeds included in the Jurassic
826 Fonzaso Fm. outcropping in the Vajont valley are the final result of a temporal sequence
827 of complex geological phenomena, including:
828 (1) initial eruption and injection into the atmosphere of volcanic ash;
829 (2) transport by wind and subsequent sedimentation in the Jurassic Vajont Basin;
830 and
831 (3) modification of the original volcanoclastic material caused by diagenesis and
832 burial-related phenomena.
833 Fine-textured volcanogenic materials were transported by wind over a long distance
834 from the explosive source (in the order of 1000–3000 km), probably from the Vardar
835 Ocean back-arc or from the Crimea (Ukraine) subduction zone, and then were deposited
836 in the Jurassic Vajont Basin.
837 Field evidence shows that:
838 (1) the oldest strata in the first 10–15 m of the cherty limestone sequence of the
839 Fonzaso Fm. (dating to middle Callovian–middle Oxfordian) do not include
840 any clay layers;
841 (2) multiple thin tephra layers concentrate in some specific 1–2 m-thick rock
842 strata sequences occurring in the upper succession of FOZ (late Oxfordian–
843 upper Tithonian) and were involved in the large basal rupture;

(3) clay layers are discontinuous (maximum ascertained continuity: 10–15 m) and can be identified, near exclusively, in some specific geological contexts: (i) the basal failure surface and (ii) the displaced and disintegrated rock mass related to the shear zone formation.

The occurrence of several distinct, very thin, clay-rich layers influenced the position of the basal failure surface of the Vajont landslide and caused its typical stepped morphology. The stratigraphic influence on the position of the basal rupture surface is strictly correlated with the occurrence of the first tephra layers within the Fonzaso Fm. In fact, the mineralogical and geochemical analyses showed that the clay layers sampled at the basal contact between the sliding surface and the shear zone were characterised by a higher content of clay minerals (Fig. 9) and had a considerable amount of illite/smectite mixed layers. Interestingly, clay layers occurring on the eastern part of the detachment surface are characterised by major percentages of clay minerals (Fig. 9) and show a higher diagenetic maturity (Table 2) when compared with clays sampled from the western failure scar. This suggests a different stratigraphic position, that is a certain difference in the geological age, of the clay layers that are located on the eastern (older strata) and western (younger strata) parts of the large basal failure surface (Fig. 3).

The mineralogical composition of the clay layers had a strong influence on their geotechnical properties, and in particular, on the value of the residual angle of internal friction (φ_{res}). In fact, clay interbeds with a large prevalence of clay minerals (CM > 79%) are characterised by low values of φ_{res} (6.7–14.9°); whereas clayey materials with a large content of granular minerals (calcite and quartz) have greater values of φ_{res} (19.5–26.7°). The mechanical role played by these soft clay interbeds in the instability

868 processes that involved the northern slope of Mt. Toc over time was different when
869 considering the prehistoric rockslide and the 1963 en-block remobilisation.
870 When considering the ancient slope failures and the primary structure of the
871 multi-layered rock mass, the occurrence of concentrated clay interbeds within some
872 specific rock strata sequences caused a localised decrease in the available shear
873 strength, enabling relative shear displacements along the dip-slope bedding planes. To
874 accommodate the deformation induced by the incipient instability condition of the
875 slope, cross-cutting fractures caused by tensile and secondary shear stresses formed
876 within the 5–10 cm-thick limestone beds, thus determining the enucleation and
877 propagation of multiple internal shear/tensile rupture surfaces. As a result, the basal
878 failure surface of the prehistoric rockslides, which was subsequently re-worked during
879 the 1963 remobilisation, had a complex stepped shape, involving several distinct clay-
880 rich layers.
881 Differently, when considering the instability process that involved the Mt. Toc
882 slope during the operating period of the hydroelectric power plant (1960–1963) and that
883 culminated with the catastrophic failure on 9 October 1963, the mechanical influence of
884 the clay layers is strictly related to the decrease in the average shear strength of the
885 previously formed basal shear zone of the slide. In fact, the basal failure mechanism of
886 the 1963 Vajont slide was complex and involved various geological materials: spread
887 bentonitic layers of variable residual shear strength, rock joints, cherty limestone beds
888 and a prevailing amount of limestone angular gravel. This means that the shear strength
889 of the basal rupture zone cannot be only related to the residual shear resistance of the
890 weakest materials, i.e. of the bentonites with a higher content of clay minerals; but the
891 shear strength of the other materials involved in the basal rupture has to be considered.

892 This also explains how a single “critical” low-resistance clay layer at the base of the
893 slide (Hendron and Patton, 1985) represents an inadequate geotechnical simplification.
894 As a whole, the 1963 Vajont landslide is an excellent case-history to learn the
895 necessity to always balance the detailed basic geological knowledge (geomorphology,
896 lithostratigraphy and structural geology) with further slope stability analyses and/or
897 advanced numerical modelling. This is true even if about 60 years are passed since the
898 catastrophic event, and that hard lesson remains valid, both for engineers and geologists.
899 Currently, the progress in the scientific research has widely proved the possible
900 occurrence of volcanoclastic clays within sedimentary sequences of Mesozoic or even
901 Paleozoic age, and this is well exemplified by some tephra levels identified thanks to a
902 lithostratigraphic field survey performed in various geological contexts around the
903 world (Huff, 2016). For this reason, the soft I/S mixed layer clays characterising the
904 base of the Vajont landslide do not represent an impossible geological contingency, as
905 thought many years ago by Müller, but rather a complex stratigraphical circumstance
906 that can be recognised only after a very accurate field survey. Analogously, the
907 occurrence of huge prehistoric landslides on alpine valleys, most of which occurred
908 after LGM or during the early Holocene, is a geological evidence that is widely
909 accepted today by the scientific community (Heim, 1932; Abele, 1974; Prager et al.,
910 2008; McColl, 2012), and the prehistoric Vajont landslide is only one example of the
911 many case-histories recorded in various geographical contexts.
912 Clay-rich interbeds within sedimentary sequences, especially those including
913 smectite and/or mixed layers clays with low shear strength, represent a typical example
914 in which a relatively minor geological feature has a major impact on the behaviour of
915 the rock mass and the related slope stability condition (e.g., Tommasi et al., 2009;
916 Esposito et al., 2013; Massey et al., 2013; Tonelli et al., 2019). As this paper

demonstrates, the genesis and geological formation processes of clay interbeds have strong influence on their geometrical shape, lithostratigraphic position in the rock sequence, mineralogical characteristics and, in turn, geotechnical properties, which exert significant controls over the slope failure mechanism and type of movement.

As concluding remark, it can be emphasised that the traditional geological field survey maintains its basic importance to adequately investigate previous landslides or slope instability processes, and this is particularly true for very complex geological situations, as the catastrophic Vajont landslide demonstrates. Sophisticated numerical modelling cannot never compensate for the poor quality of the geological investigation, and the weakness of basic knowledge or even preconceived ideas can strongly affect the correct interpretation of a rock slope stability problem.

Declaration of competing interest: The authors declare that they have no competing interests or personal relationships that could have appeared to influence the work reported in this paper.

Funding: This research received no specific grant from any funding agency in the public, commercial, or not-for-profit sectors.

Authors' contribution: Authors make substantial contributions to conception and design, and/or acquisition of data, and/or analysis and interpretation of data.

939 **References**

940 Abele, G., 1974. Bergstürze in den Alpen: ihre Verbreitung, Morphologie und
941 Folgeerscheinungen. Wissenschlaftliche Alpenvereinshefte, 25. München, 230 pp.
942 Alonso, E.E., Pinyol, N.M., 2010. Criteria for rapid sliding: I. A review of Vaiont case.
943 Engineering Geology 114, 198-210.
944 Árkai, P., 2002. Phyllosilicates in very low-grade metamorphism: transformation to
945 micas. In: Mottana, A., Sassi, F.P., Thomson, J.B., Guggenheim, S. (Eds.), Micas:
946 Crystal Chemistry and Metamorphic Petrology. Mineralogical Society of America,
947 Reviews in Mineralogy and Geochemistry 46, 463-478.
948 American Society for Testing and Materials, 1993. Standard classification of soils for
949 engineering purposes. Test Designation D2487, Volume 04.08. Available online at:
950 https://www.astm.org/Standards/D2487 (accessed on 10 July 2021).
951 Basilone, L., Morticelli, M.G., Lena, G., 2010. Mesozoic tectonics and volcanism of
952 Tethyan rifted continental margins in western Sicily. Sedimentary Geology 226, 54-
953 70.
954 Bernoulli, D., Peters, T., 1970. Traces of rhyolitic-trachytic volcanism in the Upper
955 Jurassic of the Southern Alps. Eclogae Geologicae Helvetiae 63, 609-621.
956 Berra, F., Galli, M.T., Reghellin, F., Torricelli, S., Fantoni, R., 2009. Stratigraphic
957 evolution of the Triassic-Jurassic succession in the Western Southern Alps (Italy):
958 the record of the two-stage rifting on the distal passive margin of Adria. Basin
959 Research 21, 335-353.
960 Bethke, C.M., Vergo, N., Altaner, S., 1986. Pathways of smectite illitization. Clays and
961 Clay Minerals 34 (2), 125-135.

962 Bhatia, M.R., Crook, K.A.W., 1986. Trace element characteristics of graywackes and
963 tectonic setting discrimination of sedimentary basins. Contrib. Mineral. Petrol. 92,
964 181-193.
965 Bolla, A., Paronuzzi, P., Pinto, D., Lenaz, D., Del Fabbro, M., 2020. Mineralogical and
966 geotechnical characterization of the clay layers within the basal shear zone of the
967 1963 Vajont landslide. Geosciences 10 (9), 360.
968 Bonev, N., Stampfli, G., 2008. Petrology, geochemistry and geodynamic implications of
969 Jurassic island arc magmatism as revealed by mafic volcanic rocks in the Mesozoic
970 low-grade sequence, eastern Rhodope, Bulgaria. Lithos 100, 210-233.
971 Broili, L., 1967. New knowledges on the geomorphology of the Vaiont slide slip
972 surfaces. Rock Mechanics and Engineering Geology 5, 38-88.
973 Casagrande, A., 1948. Classification and identification of soils. Trans. ASCE 113, 901-
974 991.
975 Christidis, G., Dunham, A.C., 1993. Compositional variations in smectites: part I.
976 Alteration of intermediate volcanic rocks. A case study from Milos Island, Greece.
977 Clay Minerals 28, 255-273.
978 Compton, J.S., 1991. Origin and diagenesis of clay minerals in the Monterey Formation,
979 Santa Maria basin area, California. Clays and Clay Minerals 39, 449-466.
980 Cuadros, J., Altaner, S., 1998. Characterization of mixed-layer illite-smectite from
981 bentonites using microscopic, chemical and X-ray methods: Constraints on the
982 smectite-to-illite transformation mechanism. American Mineralogist 83, 762-774.
983 Dykes, A.P., Bromhead, E.N., 2018. The Vaiont landslide: re-assessment of the
984 evidence leads to rejection of the consensus. Landslides 15, 1815-1832.
985 Eslinger, E., Pevear, D.R., 1988. Clay minerals for petroleum geologists and engineers.
986 SEPM Short Course No. 22, Society for Sedimentary Geology, Tulsa, USA, 428 pp.

987 Esposito, C., Bianchi-Fasani, G., Martino, S., Scarascia-Mugnozza, G., 2013.
988 Quaternary gravitational morpho-genesis of Central Apennines (Italy): Insights from
989 the Mt. Genzana case history. Tectonophysics 605, 96-103.
990 Fang, Q., Churchman, G.J., Hong, H., Chen, Z., Liu, J., Yu, J., Han, W., Wang, C.,
991 Zhao, L., Furnes, H., 2017. New insights into microbial smectite illitization in the
992 Permo-Triassic boundary K-bentonites, South China. Applied Clay Science 140, 96-
993 111.
994 Ferri, F., Di Toro, G., Hirose, T., Han, R., Noda, H., Shimamoto, T., Quaresimin, M., de
995 Rossi, N., 2011. Low- to high-velocity frictional properties of the clay-rich gouges
996 from the slipping zone of the 1963 Vaiont slide, northern Italy. Journal of
997 Geophysical Research 116, B09208, doi:10.1029/2011JB008338.
998 Fiore, S., 1993. The occurrences of smectite and illite in a pyroclastic deposits prior to
999 weathering: implications on the genesis of 2:1 clay minerals in volcanic soils.
1000 Applied Clay Science 8, 249-259.
1001 Giudici, F., Semenza, E., 1960. Studio geologico sul serbatoio del Vajont. Unpublished
1002 report for SADE, Venezia, Italy. 63 pp.
1003 Heim, A., 1932. Bergsturz und Menschenleben. Zürich Fretz & Wasmuth Verlag.,
1004 Zürich, 218 pp. In German.
1005 Hein, J.R., Koski, R.A., Morgenson, L.A., 1982. Uranium and thorium enrichment in
1006 rocks from the base of DSDP Hole 465A, Hess Rise, central North Pacific.
1007 Chemical Geology 36, 237-251.
1008 Hendron, A.J., Patton, F.D., 1985. The Vaiont slide, a geotechnical analysis based on
1009 new geologic observations of the failure surface. Technical Report GL-85-5,
1010 Department of the Army, U.S. Army Corps of Engineers, Washington, DC.

1011 Hesselbo, S.P., Robinson, S.A., Surlyk, F., Piasecki, S., 2002. Terrestrial and marine
1012 extinction at the Triassic-Jurassic boundary synchronized with major carbon-cycle
1013 perturbation: A link to initiation of massive volcanism? Geology 30, 251-254.
1014 Hesselbo, S.P., Jenkyns, H.C., Duarte, L.V., Oliveira, L.C.V., 2007. Carbon-isotope
1015 record of the Early Jurassic (Toarcian) Oceanic Anoxic Event from fossil wood and
1016 marine carbonate (Lusitanian Basin, Portugal). Earth and Planetary Science Letters
1017 253, 455-470.
1018 Huang, W.-L., Longo, J.M., Pevear, D.R., 1993. An experimentally derived kinetic
1019 model for smectite-to-illite conversion and its use as a geothermometer. Clays and
1020 Clay Minerals 41, 162-177.
1021 Huff, W.D., 2016. K-bentonites: A review. American Mineralogist 101, 43-70.
1022 Inoue, A., Lanson, B., Marques-Fernandes, M., Sakharov, B.A., Murakami, T.,
1023 Meunier, A., Beaufort, D., 2005. Illite-smectite mixed-layer minerals in the
1024 hydrothermal alteration of volcanic rocks: I. One-dimensional XRD structure
1025 analysis and characterization of component layers. Clays and Clay Minerals 53 (5),
1026 423-439.
1027 Kelepertsis, A.E., 1981. The geochemistry of uranium and thorium in some Lower
1028 Carboniferous sedimentary rocks (Great Britain). Chemical Geology 34, 275-288.
1029 Kenney, T.C., 1967. The influence of mineral composition on the residual strength of
1030 natural soils. Proceedings of Geotechnical Conference. Oslo(1), pp. 123-129.
1031 Kenney, T.C., 1992. Slope stability in artificial reservoirs: influence of reservoir level,
1032 selected cases, and possible solutions. In: Semenza, E., Melidoro, G. (Eds.),
1033 Proceedings of the meeting on the 1963 Vaiont landslide, 17-19 September 1986,
1034 Ferrara, Cansiglio and Vaiont. Grafica Ferrarese, Ferrara, Italy, pp 67-85.
1035 Kiersch, G.A., 1964. Vaiont reservoir disaster. Civil Engineering 34, 32-39.

1036 Lanson, B., Sakharov, B.A., Claret, F., Drits, V.A., 2009. Diagenetic illite-to-smectite
1037 transition in clay-rich sediments: a reappraisal of x-ray diffraction results using the
1038 multi-specimen method. American Journal of Science 309, 476-516.
1039 Latin, D., Waters, F., 1992. Basaltic magmatism in the North Sea and its relationship to
1040 lithospheric extension. Tectonophysics 208, 77-90.
1041 Lenaz, D., Schmitz, B., Alvarez, W., 2019. Terrestrial Cr-spinels in the Maiolica
1042 limestone: Where are they from? In: Koeberl, C., Bice, D.M. (Eds.), 250 Million
1043 Years of Earth History in Central Italy: Celebrating 25 Years of the Geological
1044 Observatory of Coldigioco: Geological Society of America Special Paper 542, pp.
1045 121-131.
1046 Lo, K.Y., Lee, C.F., Gélinas, P., 1972. Alternative interpretation of the Vaiont slide. In:
1047 Cording, E.J. (Ed.), Stability of Rock Slopes. Proc. 13th Symp. on Rock Mechanics,
1048 Univ. Illinois, Urbana. ASCE, New York, pp. 595-623.
1049 Mantovani, F., Vita-Finzi, C., 2003. Neotectonics of the Vajont dam site.
1050 Geomorphology 54, 33-37.
1051 Martinis, B., 1978. Contributo alla stratigrafia dei dintorni di Erto-Casso (Pordenone) ed
1052 alla conoscenza delle caratteristiche strutturali e meccaniche della frana del Vajont.
1053 Memorie di Scienze Geologiche Università di Padova 32, 1-33.
1054 Masè, G., Semenza, M., Semenza, P., Semenza, P., Turrini, M.C., 2004. Le foto della
1055 frana del Vajont. Edizioni k-flash, Ferrara, Italy (3 maps and CD-ROM, 650 MB).
1056 Massey, C.I., Petley, D.N., McSavaney, M.J., 2013. Patterns of movement in
1057 reactivated landslides. Engineering Geology 159, 1-19.
1058 McColl, S.T., 2012. Paraglacial rock-slope stability. Geomorphology 153-154, 1-16.
1059 Meijers, M.J.M., Vrouwe, B., van Hinsbergen, D.J.J., Kuiper, K.F., Wijbrans, J.,
1060 Davies, G.R., Stephenson, R.A., Kaymak, N., Matenco, L., Saintot, A., 2010.

1061 Jurassic arc volcanism on Crimea (Ukraine): Implications for the paleo-subduction
1062 zone configuration of the Black Sea region. Lithos 119, 412-426.
1063 Merriman, R.J., 2005. Clay minerals and sedimentary basin history. European Journal
1064 of Mineralogy 17, 7-20.
1065 Merriman, R.J., Peacor, D.R., 1999. Very low-grade metapelites: mineralogy,
1066 microfabrics and measuring reaction progress. In: Frey, M., Robinson, D. (Eds.),
1067 Low-Grade Metamorphism, Blackwell Science, Oxford, pp. 10-60.
1068 Mirabella, A., Egli, M., Raimondi, S., Giaccai, D., 2005. Origin of clay minerals in soils
1069 on pyroclastic deposits in the island of Lipari (Italy). Clays and Clay Minerals 53(4),
1070 409-421.
1071 Mizota, C., Faure, K., 1998. Hydrothermal origin of smectite in volcanic ash. Clays and
1072 Clay Minerals 46(2), 178-182.
1073 Moore, D.M., Reynolds, R.C. Jr. 1997. X-ray diffraction and the identification and
1074 analysis of clay minerals, 2nd edition. Oxford University Press, New York, 332 pp.
1075 Müller, L., 1964. The rock slide in the Vajont valley. Rock Mechanics and Engineering
1076 Geology 2, 148-212.
1077 Müller, L., 1968. New considerations on the Vaiont slide. Rock Mechanics and
1078 Engineering Geology 6, 1-91.
1079 Murray, H.H., 2006. Applied Clay Mineralogy. Occurrences, Processing and
1080 Applications of Kaolins, Bentonites, Palygorskitesepiolite, and Common Clays.
1081 Elsevier Science, 188 pp.
1082 Nonveiller, E., 1967. Shear strength of bedded and jointed rock as determined from the
1083 Zalesina and Vajont slides. Proceedings of Geotechnical Conference, Oslo, Norway.
1084 Norwegian Geotechnical Institute 1, pp. 289-294.

1085 Paronuzzi, P., Bolla, A., 2012. The prehistoric Vajont rockslide: an updated geological
1086 model. Geomorphology 169-170, 165-191.
1087 Paronuzzi, P., Bolla, A., 2013. A new interpretation of the geotechnical context of the
1088 Vajont rockslide. In: Margottini, C., Canuti, P., Sassa, K. (Eds.), Landslide Science
1089 and Practice: Risk Assessment, Management and Mitigation. Proceedings of the
1090 Second World Landslide Forum, 3-9 October 2011, Rome, Italy. Springer, Berlin,
1091 Germany, pp. 123-132.
1092 Paronuzzi, P., Bolla, A., 2015a. Gravity-induced rock mass damage related to large en
1093 masse rockslides: evidence from Vajont. Geomorphology 234, 28-53.
1094 Paronuzzi, P., Bolla, A., 2015b. Gravity-induced fracturing in large rockslides: possible
1095 evidence from Vajont. In: Lollino, G., Giordan, D., Crosta, G.B., Corominas, J.,
1096 Azzam, R., Wasowski, J., Sciarra, N. (Eds.), Engineering Geology for Society and
1097 Territory: Landslide Processes. Proceedings of the XII International IAEG
1098 Congress, 15-19 September 2014, Turin, Italy. Springer, pp. 213-216.
1099 Paronuzzi, P., Rigo, E., Bolla, A., 2013a. Influence of filling–drawdown cycles of the
1100 Vajont reservoir on Mt. Toc slope stability. Geomorphology 191, 75-93.
1101 Paronuzzi, P., Rigo, E., Bolla, A., 2013b. A coupled seepage-stability model to analyze
1102 the Vajont reservoir influence. In: Margottini, C., Canuti, P., Sassa, K. (Eds.),
1103 Landslide Science and Practice: Risk Assessment, Management and Mitigation.
1104 Proceedings of the Second World Landslide Forum, 3-9 October 2011, Rome, Italy.
1105 Springer, Berlin, Germany, pp. 97-106.
1106 Paronuzzi, P., Bolla, A., Rigo, E., 2016. Brittle and ductile behavior in deep-seated
1107 landslides: learning from the Vajont experience. Rock Mechanics and Rock
1108 Engineering 49 (6), 2389-2411.

1109 Pellenard, P., Deconinck, J.-F., Huff, W.D., Thierry, J., Marchand, D., Fortwengler, D.,
1110 Trouiller, A., 2003. Characterization and correlation of Upper Jurassic (Oxfordian)
1111 bentonite deposits in the Paris Basin and the Subalpine Basin, France.
1112 Sedimentology 50, 1035-1060.
1113 Pellenard, P., Nomade, S., Martire, L., De Oliveira Ramalho, F., Monna, F., Guillou, H.,
1114 2013. The first 40Ar–39Ar date from Oxfordian ammonite-calibrated volcanic
1115 layers (bentonite) as a tie-point for the Late Jurassic. Geological Magazine 150(6),
1116 1136-1142.
1117 Prager, C., Zangerl, C., Patzelt, G., Brandner, R., 2008. Age distribution of fossil
1118 landslides in the Tyrol (Austria) and its surrounding areas. Natural Hazards and
1119 Earth System Sciences 8, 377-407.
1120 Pytte, A.M., Reynolds, R.C., 1989. The thermal transformation of smectite to illite. In:
1121 Naeser, N.D., McCulloh, T.H. (Eds.), Thermal History of Sedimentary Basins,
1122 Springer-Verlag, Berlin, pp. 133-140.
1123 Quirie, A.K., Schofield, N., Hartley, A., Hole, M.J., Archer, S.G., Underhill, J.R.,
1124 Watson, D., Holford, S.P., 2019. The Rattray Volcanics: Mid-Jurassic fissure
1125 volcanism in the UK Central North Sea. Journal of the Geological Society 176, 462-
1126 481.
1127 Selli, R., Trevisan, L., 1964. Caratteri e interpretazione della Frana del Vaiont. Giornale
1128 di Geologia 32, 7–104.
1129 Spinola, D.S., Pi-Puig, T., Solleiro-Rebolledo, E., Egli, M., Sudo, M., Sedov, S., Kűhn,
1130 P., 2017. Origin of clay minerals in Early Eocene volcanic palaeosols on King
1131 Gorge Island, Maritime Antarctica. Nature, Scientific Reports 7, 6368,
1132 doi:10.1038/s41598-017-06617-x.

1133 Tika, T.h.E., Hutchinson, J.N., 1999. Ring shear tests on soil from the Vaiont slide slip
1134 surface. Géotechnique 49(1), 59-74.
1135 Tommasi, P., Verrucci, L., Campedel, P., Veronese, L., Pettinelli, E., Ribacchi, R.,
1136 2009. Buckling of high natural scope: The case of Lavini di Marco (Trento-Italy).
1137 Engineering Geology 109, 93-108.
1138 Tonelli, G., Veneri, F., Mattioli, M., Paletta, C., 2019. The role of a bentonitic layer on
1139 slope stability in bedded limestone: The case study of the December 2004 Ca'
1140 Madonna Quarry rock slide (Umbria-Marche Apennines, Central Italy). Italian
1141 Journal of Geosciences 138, 56-65.
1142 Velde, B., 1995. Origin and Mineralogy of Clays. Clays and the Environment. Springer-
1143 Verlag, 334 pp.
1144 Wang, B.-Q., Wang, W., Zhou, M.F., 2013. Provenance and tectonic setting of the
1145 Triassic Yidun Group, the Yidun Terrane, Tibet. Geosci. Front. 4, 765-777.
1146 Weibel, R., 1999. Effects of burial on the clay assemblages in the Triassic Skagerrak
1147 Formation, Denmark. Clay Minerals 34, 619-635.
1148 Winchester, J.A., Floyd, P.A., 1977. Geochemical discrimination of different magma
1149 series and their differentiation products using immobile elements. Chem. Geol. 20,
1150 325-343.
1151 Wolter, A., Stead, D., Clague, J.J., 2014 A morphological characterisation of the 1963
1152 Vajont Slide, Italy, using long-range terrestrial photogrammetry. Geomorphology
1153 206, 147-164.
1154 Wolter, A., Stead, D., Ward, B.C., Clague, J.J., Ghirotti, M., 2016. Engineering
1155 geomorphological characterisation of the Vajont Slide, Italy, and a new
1156 interpretation of the chronology and evolution of the landslide. Landslides 13, 1067-
1157 1081.

1158 Zhang, Y., Pe-Piper, G., Piper, D.J.W., 2013. Sediment geochemistry as a provenance
1159 indicator: Unravelling the cryptic signatures of polycyclic sources, climate change,
1160 tectonism and volcanism. Sedimentology 61, 383-410.
1161 Ziegler, P.A., 1990. Geological Atlas of Western and Central Europe. 2nd Edition, Shell
1162 International Petroleum Mij. B.V. and Geological Society, London, 239 pp.
1163

Figure captions

Fig. 1. Aerial view of the Vajont dam area shortly after the disaster that occurred on 9 October 1963, showing the 300 Mm^3 landslide mass that filled the artificial reservoir. This picture (available at https://www.ilpost.it/2013/10/09/il-disastro-del-vajont/vajont-dam/, Copyright holder: Associated Press Photo) was taken on 16 November 1963 and is one of the first colour pictures of the Vajont landslide after the catastrophe.

Fig. 2. Basal clay interbed as exhumed by Hendron and Patton during their field work on the failure surface; location 18-9 is close to VA15-166 of this study (photo modified from Hendron and Patton, 1985).

Fig. 3. Shaded relief map of the 1963 Vajont landslide and its surroundings showing the remnants of the basal shear zone resting on the detachment surface, along with the locations and identification numbers of the clays samples.

Fig. 4. Lithostratigraphic columns of both sides of the Vajont valley. The locations and identification numbers of the clay samples are as shown.

Fig. 5. (a) Rock outcrop (top of the Fonzaso Fm.) on the north valley side from which 5 clay layers were sampled, and (b) its schematisation. For the sampling location see Fig. 3.

Fig. 6. Stepped morphology of the basal failure surface characterising (a) the eastern part and (b) the western part of the detachment surface of the Vajont landslide. (c), (d) Details of a lateral step and multiple transverse steps, respectively, showing the in-situ lithostratigraphic sequence outcropping on the failure surface (Fonzaso Fm.).

Fig. 7. Clayey materials involved in the 1963 Vajont landslide and occurring: (a), (b) at the basal contact with the sliding surface; (c), (d) within a displaced and stratified

1189 rock mass; and (e), (f) within the debris of the landslide shear zone. Sample
1190 locations shown in Fig. 3.
1191 **Fig. 8.** Field sampling and XRPD patterns of (a)-(b) clay-rich sample VA07-11A, and
1192 (c)-(d) calcite-rich sample VA07-3B. For the sample locations see Fig. 3.
1193 **Fig. 9.** (a) Ternary diagram showing the relative amount of clay minerals (CM), calcite
1194 (Cal) and quartz (Qtz) within the studied samples. (b) Diagram showing the
1195 relationship between the amount of clay minerals and K_2O content of the Vajont
1196 clays. Samples with red labels were collected from the eastern detachment
1197 surface, whereas samples with black labels come from the western part of the
1198 failure scar.
1199 **Fig. 10.** Rb vs. K_2O chart. The two lines show the mica-trend (above) and the feldspar-
1200 trend (below) according to Zhang et al. (2013).
1201 **Fig. 11.** (a) Th-Co-Zr/10 ternary diagram for the studied samples. Fields after Bhatia
1202 and Crook (1986). (b) Zr/Ti vs. Nb/Y diagram for the analysed clay samples from
1203 Vajont (red circles). The bentonite layers analysed by Pellenard et al. (2013) are
1204 also shown (blue field and circles). Fields after Winchester and Floyd (1977).
1205 **Fig. 12.** Comparative spidergrams of trace elements for different materials with a
1206 possible common provenance. Fields are displayed considering minimum and
1207 maximum contents of the trace elements for each dataset.
1208 **Fig. 13** Plasticity chart of some selected clay samples exhumed from different
1209 geological contexts related to the Vajont landslide (modified from Bolla et al.,
1210 2020).
1211 **Fig. 14** Correlation diagrams of some Vajont clay samples exhumed from different
1212 geological contexts, showing (a) liquid limit vs. clay mineral content and (b)
1213 residual friction angle vs. clay mineral content.

Table 1
Mineralogical composition and values of the residual angle of internal friction of clayey materials sampled from the Vajont slide, according to different Authors.

Author (Year)	No. of samples analysed	Mineralogical composition	Residual angle of internal friction
Broili (1967)[a]	Not mentioned	8–30% clay minerals (Montmorillonite, Illite)	–
Kenney (1967)	3	Montmorillonite (25–75%) Illite (5–30%) Calcite (7–40%) Quartz (5–10%) Feldspar (0–5%)	9–16°
Nonveiller (1967)	Unknown	–	5–7°
Hendron and Patton (1985)	3	50–80% clay minerals (Montmorillonite 25–75%, Vermiculite/Smectite, Illite, Corrensite, Kaolinite), Calcite, Quartz	5–16°
Tika and Hutchinson (1999)	2	Smectite (0–25%) Illite/Smectite (25–50%) Kaolinite (< 5%) Calcite (40–45%) Quartz (< 10%)	9–11° (low-velocity)
Ferri et al. (2011)	1	Smectite (60–70%) Calcite (20–30%) Quartz (< 5%)	24–26° at 40–60% humidity 8–10° at water saturation (low-velocity)
Bolla et al. (2020)	9	Illite/Smectite (36–96%) Calcite (4–64%) Quartz (< 6%)	7–15° for clay-rich samples 20–27° for calcite-rich samples

[a] Interbeds of pelitic materials (limey marl and marly limestone).

Table 2
Geological context, mineralogical composition and calcite content of selected clay samples (< 2 μm fraction) from Vajont (modified from Bolla et al., 2020).

Sample	Geological context	Reichweite[d]	Illite percentage[d]	Clay minerals[e] [wt. %]	Calcite[e] [wt. %]	Quartz[e] [wt. %]	$CaCO_3$ from calcimetry [wt. %]
VA07-3A[a]	Disintegrated rock mass	*R*0, *R*1	50–60%, 60–70%	83	17	< 1	29
VA07-3B	Disintegrated rock mass	*R*0, *R*1	n.d.	59	39	3	43
VA07-8[a]	Disintegrated rock mass	*R*0, *R*1	50–60%, 70–80%	60	34	6	41
VA09-1A	In-situ sequence	*R*0, *R*1	50–60%, 80–85%	79	19	2	19
VA09-1B	In-situ sequence	*R*0, *R*1	50–60%, 80–85%	89	10	1	18
VA07-5A[b]	Displaced rock mass	*R*1, *R*0	60–70% and 80–85%, 50%	36	64	< 1	66
VA07-11A	Displaced rock mass	*R*1, *R*0	60–70%, 50%	90	9	1	12
VA07-13C	Basal contact	*R*1	70–80%	79	17	4	23
VA07-14[c]	Basal contact	*R*1	70–80%	96	4	0	5

[a] Kaolinite and illite as traces (not determined).

[b] Kaolinite as traces (not determined).

[c] Feldspars as traces (not determined).

[d] Determined according to the criteria described in Moore and Reynolds (1997).

[e] Estimated by measuring peak areas in the diffractograms, as described in Bolla et al. (2020).

Table 3
Content of trace elements (parts-per-million) from XRF analysis of selected Vajont clay samples.

Sample	Elements [ppm]																		
	V	Cr	Co	Ni	Cu	Zn	Ga	Rb	Sr	Y	Zr	Nb	Ba	La	Ce	Nd	Pb	Th	U
VA07-3A	14	< 6	16	78	44	122	21	47	156	16	114	7	104	24	39	43	44	30	6
VA07-3B	16	13	14	58	41	81	20	33	117	20	77	14	83	13	32	41	42	28	< 3
VA07-5A	25	8	22	129	109	145	13	79	198	47	78	4	199	42	33	51	22	25	5
VA07-6	8	< 6	19	81	109	125	24	63	73	18	261	8	137	11	19	44	48	13	8
VA07-8	15	< 6	17	64	39	100	17	51	89	24	78	13	118	34	47	44	47	23	< 3
VA07-11A	< 5	8	24	181	76	221	26	102	78	12	232	4	147	< 10	14	35	40	15	6
VA07-13C	18	< 6	22	123	65	179	25	111	46	15	147	7	142	18	27	38	44	26	7
VA07-14	< 5	6	7	101	53	153	28	134	27	15	270	5	135	< 10	< 10	30	28	17	7
VA09-1A	24	< 6	39	123	88	158	24	80	43	25	228	9	88	< 10	< 10	35	33	17	6
VA09-1B	6	< 6	38	222	42	162	29	56	37	9	106	18	56	37	37	35	80	34	7

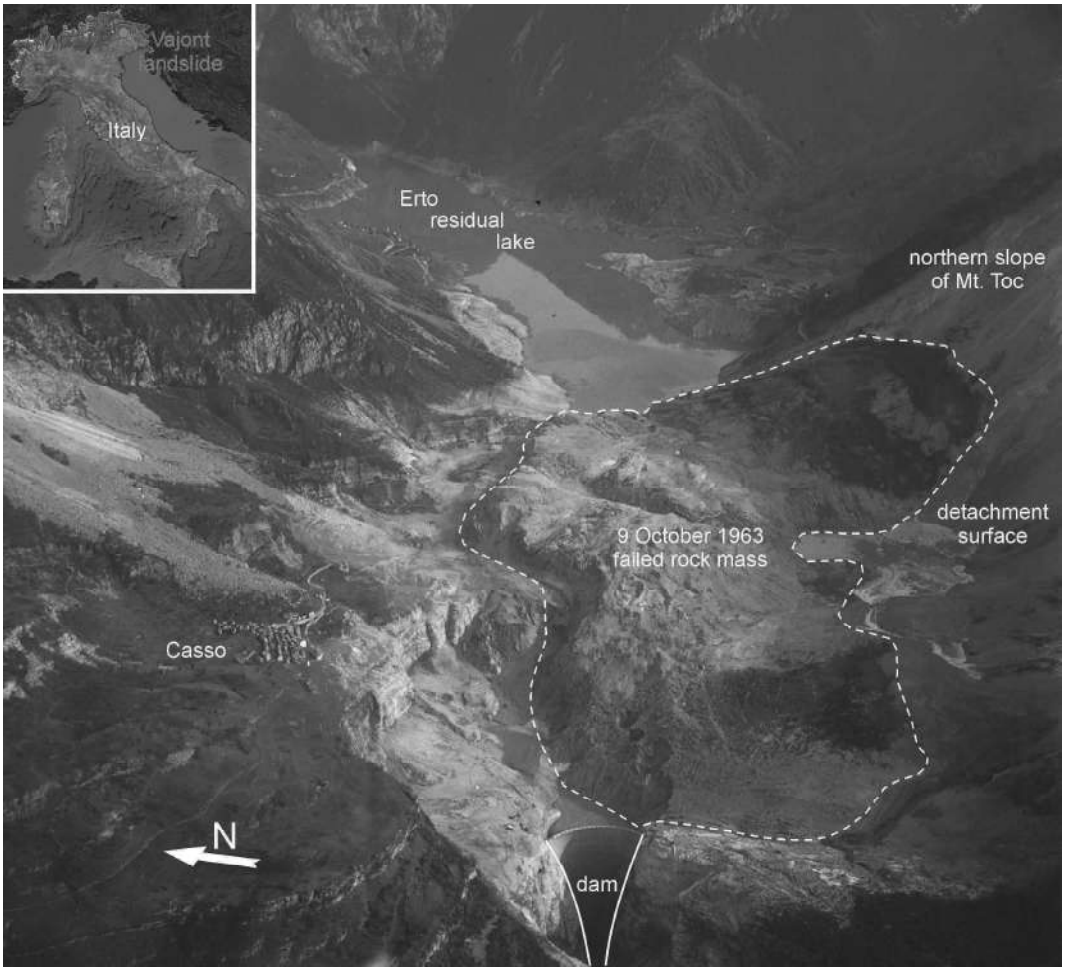

Fig. 1 500 dpi. Aerial view of the Vajont dam area shortly after the disaster that occurred on 9 October 1963, showing the 300 Mm^3 landslide mass that filled the artificial reservoir. This picture (available at https://www.ilpost.it/2013/10/09/il-disastro-del-vajont/vajont-dam/, Copyright holder: Associated Press Photo) was taken on 16 November 1963 and is one of the first colour pictures of the Vajont landslide after the catastrophe.

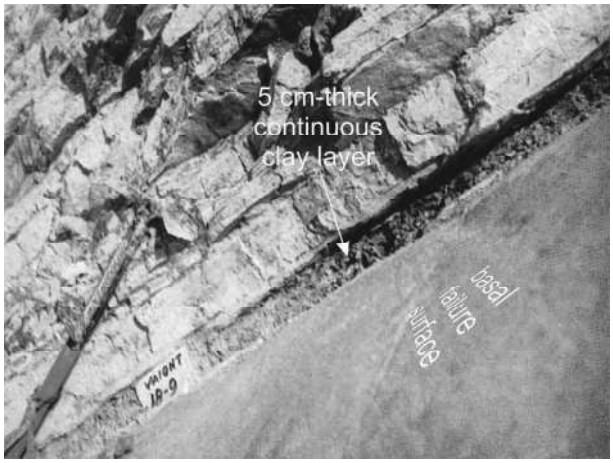

Fig. 2 700 dpi. Basal clay interbed as exhumed by Hendron and Patton during their field work on the failure surface; location 18-9 is close to VA15-166 of this study (photo modified from Hendron and Patton, 1985).

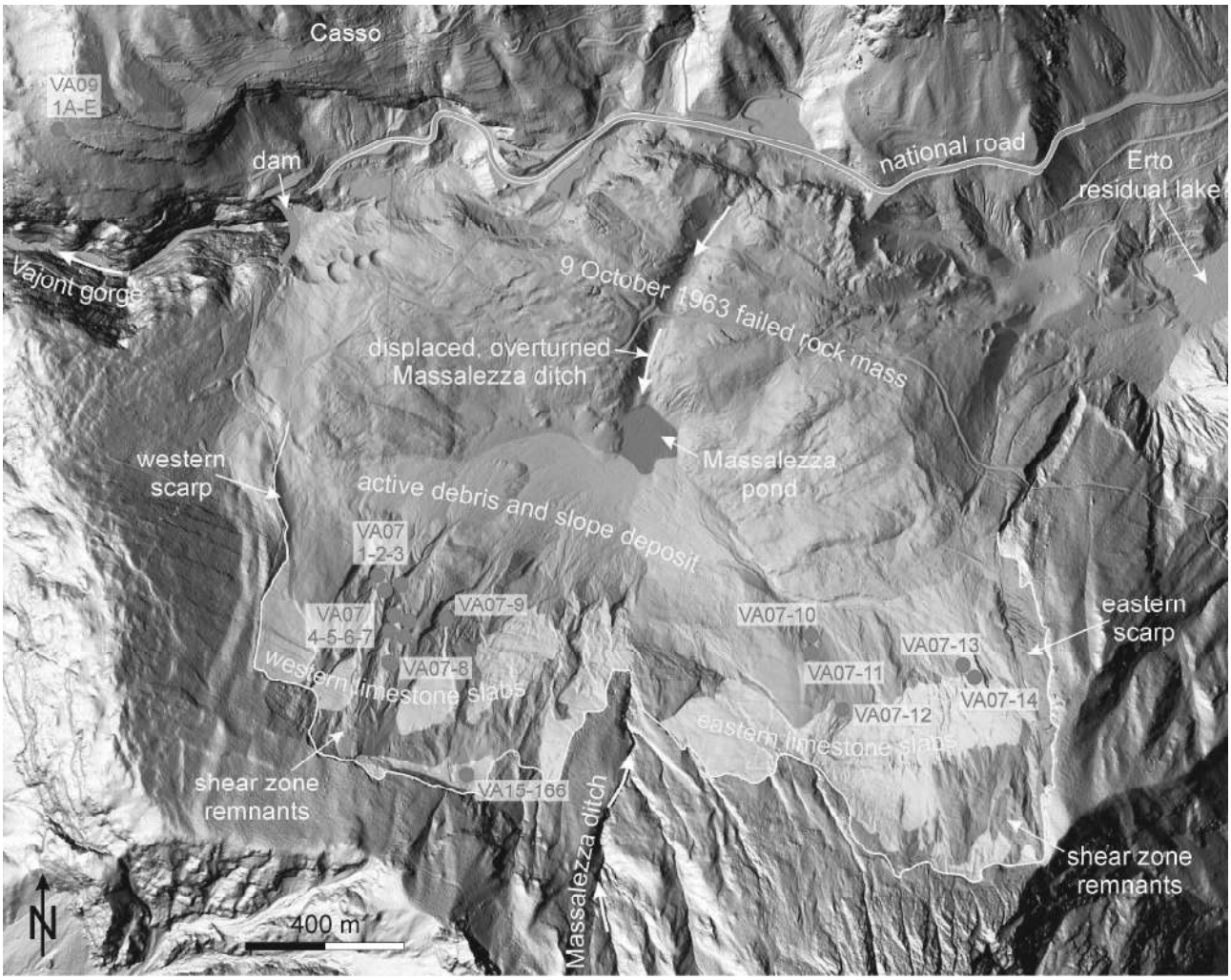

Fig. 3 500 dpi. Shaded relief map of the 1963 Vajont landslide and its surroundings showing the remnants of the basal shear zone resting on the detachment surface, along with the locations and identification numbers of the clays samples.

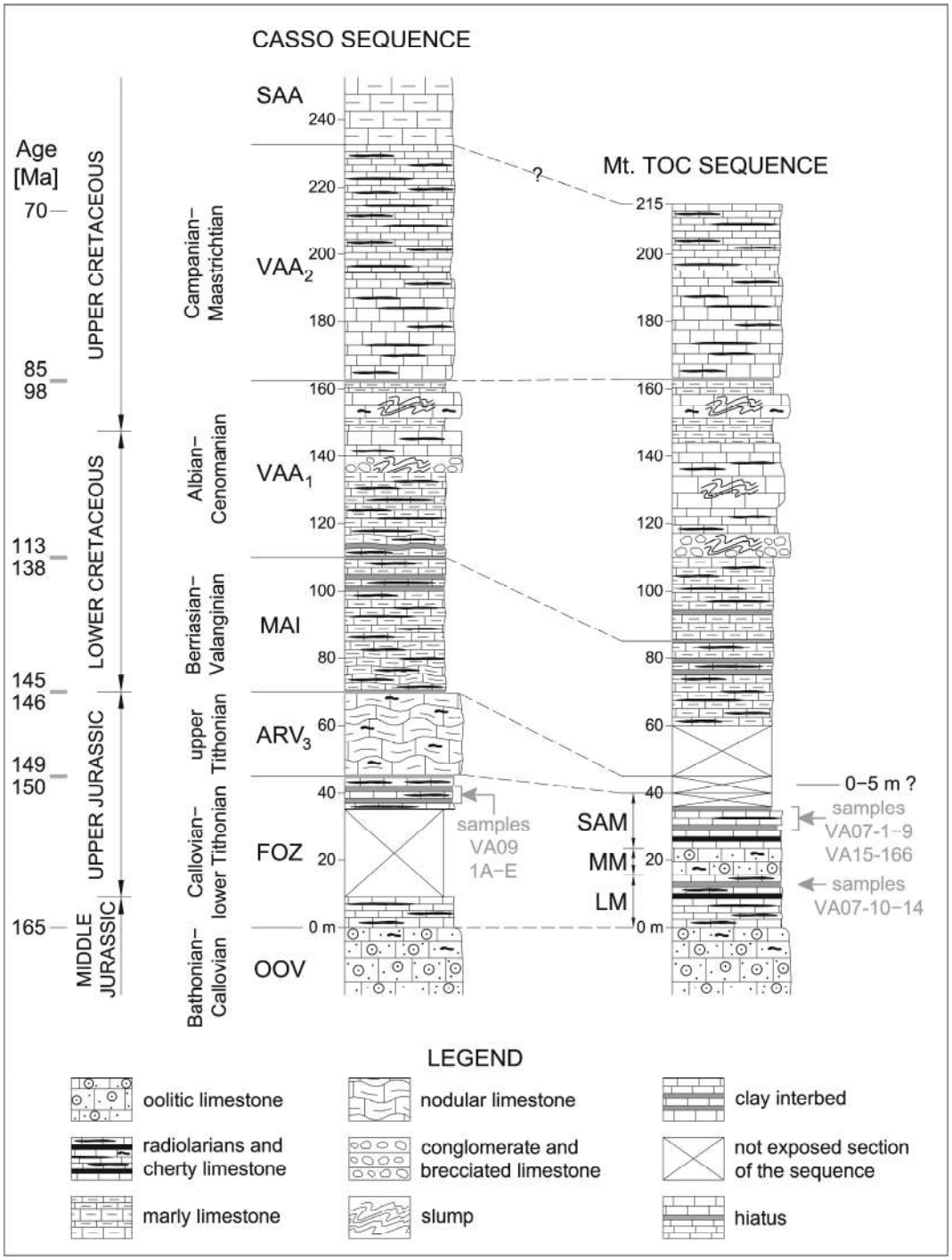

Fig. 4 1200 dpi. Lithostratigraphic columns of both sides of the Vajont valley. The locations and identification numbers of the clay samples are as shown.

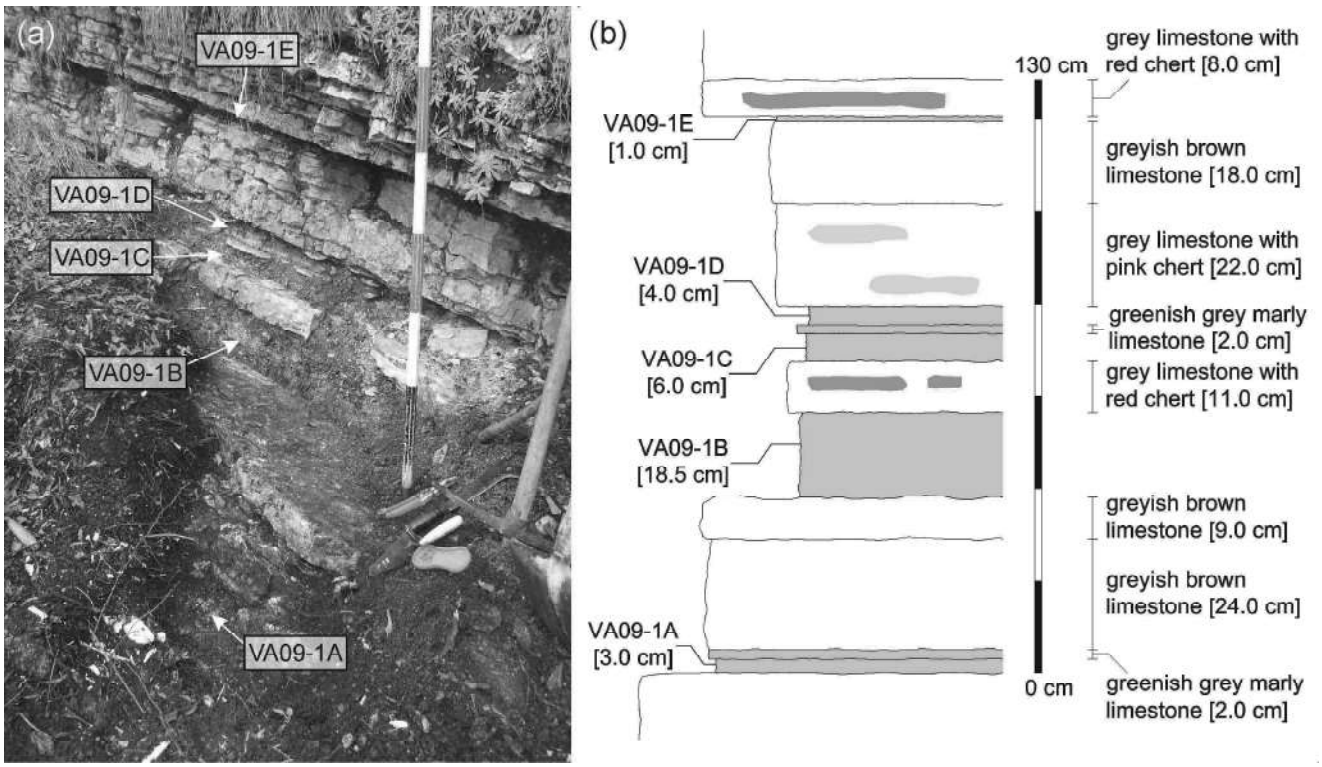

Fig. 5 500 dpi. (a) Rock outcrop (top of the Fonzaso Fm.) on the north valley side from which 5 clay layers were sampled, and (b) its schematisation. For the sampling location see Fig. 3.

Fig. 6 300 dpi. Stepped morphology of the basal failure surface characterising (a) the eastern part and (b) the western part of the detachment surface of the Vajont landslide. (c), (d) Details of a lateral step and multiple transverse steps, respectively, showing the in-situ lithostratigraphic sequence outcropping on the failure surface (Fonzaso Fm.).

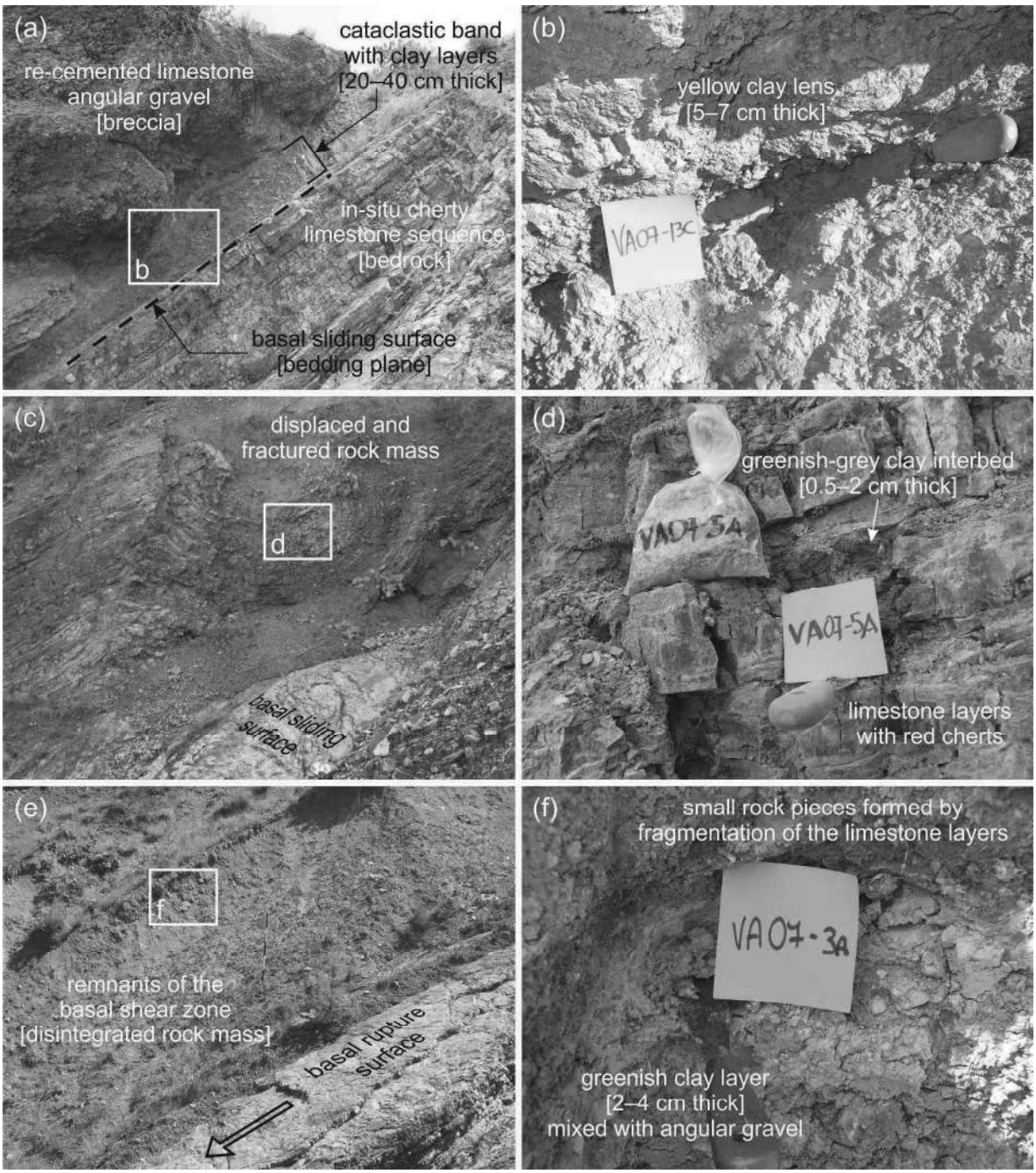

Fig. 7 300 dpi. Clayey materials involved in the 1963 Vajont landslide and occurring: (a), (b) at the basal contact with the sliding surface; (c), (d) within a displaced and stratified rock mass; and (e), (f) within the debris of the landslide shear zone. Sample locations shown in Fig. 3.

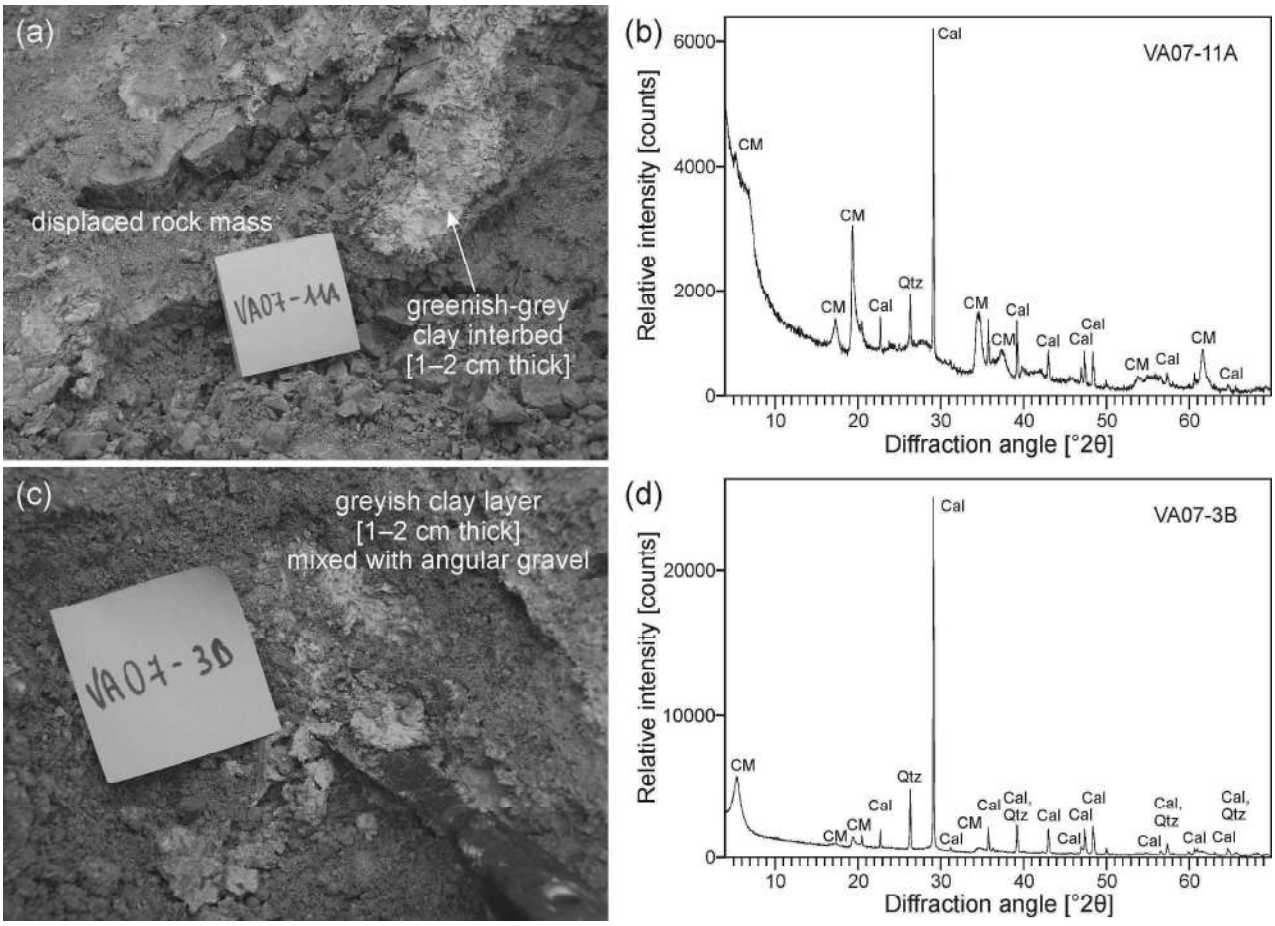

Fig. 8 500 dpi. Field sampling and XRPD patterns of (a)-(b) clay-rich sample VA07-11A, and (c)-(d) calcite-rich sample VA07-3B. For the sample locations see Fig. 3.

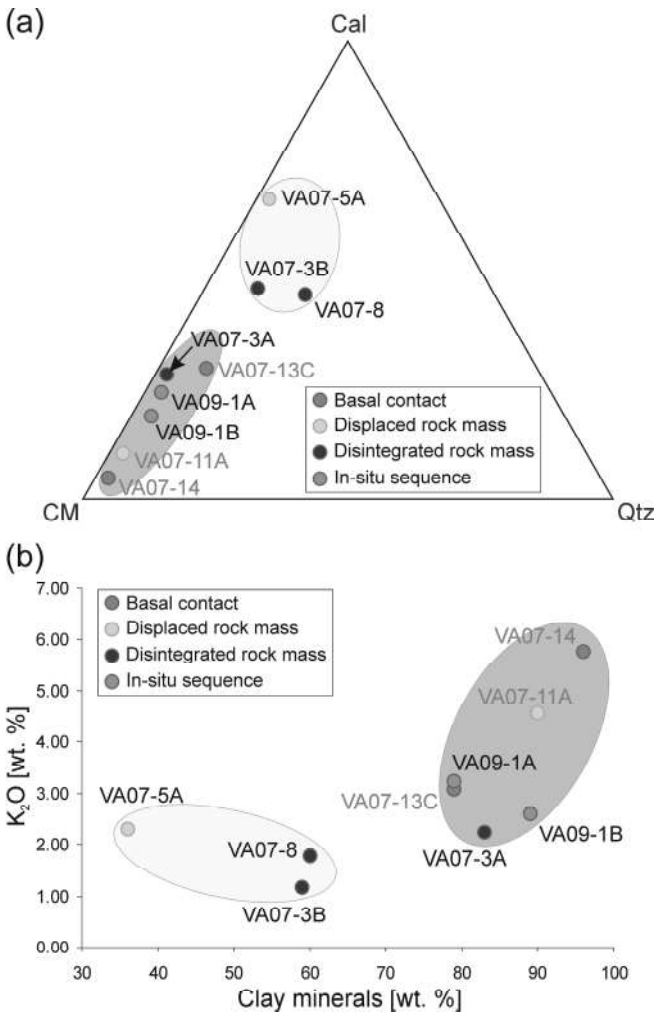

Fig. 9 1200 dpi. (a) Ternary diagram showing the relative amount of clay minerals (CM), calcite (Cal) and quartz (Qtz) within the studied samples. (b) Diagram showing the relationship between the amount of clay minerals and K_2O content of the Vajont clays. Samples with red labels were collected from the eastern detachment surface, whereas samples with black labels come from the western part of the failure scar.

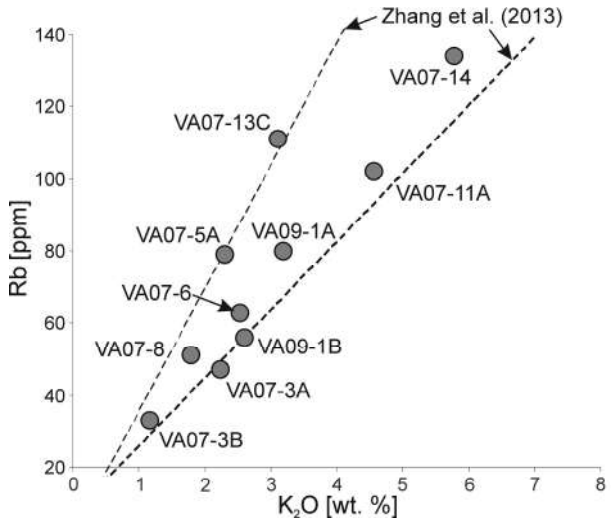

Fig. 10 1200 dpi. Rb vs. K_2O chart. The two lines show the mica-trend (above) and the feldspar-trend (below) according to Zhang et al. (2013).

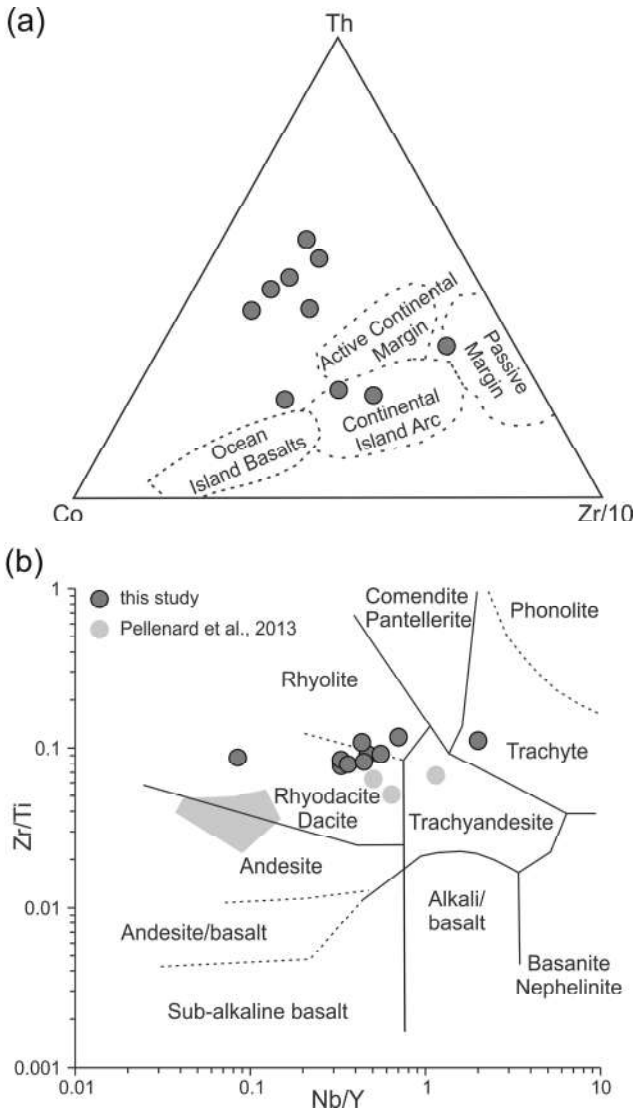

Fig. 11 1200 dpi. (a) Th-Co-Zr/10 ternary diagram for the studied samples. Fields after Bhatia and Crook (1986). (b) Zr/Ti vs. Nb/Y diagram for the analysed clay samples from Vajont (red circles). The bentonite layers analysed by Pellenard et al. (2013) are also shown (blue field and circles). Fields after Winchester and Floyd (1977).

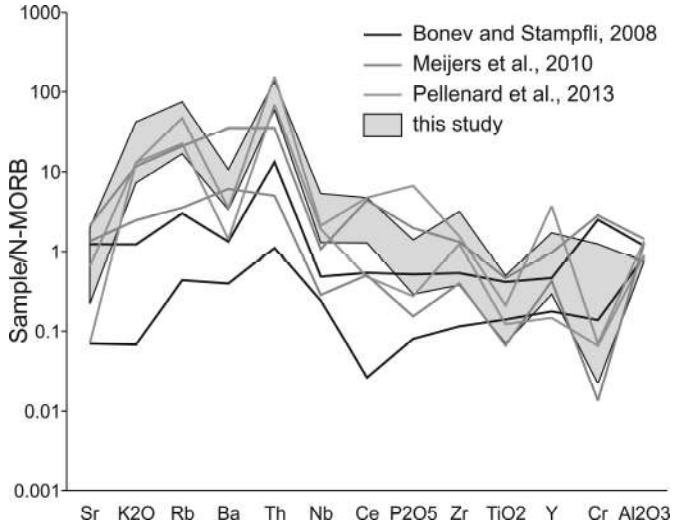

Fig. 12 1200 dpi. Comparative spidergrams of trace elements for different materials with a possible common provenance. Fields are displayed considering minimum and maximum contents of the trace elements for each dataset.

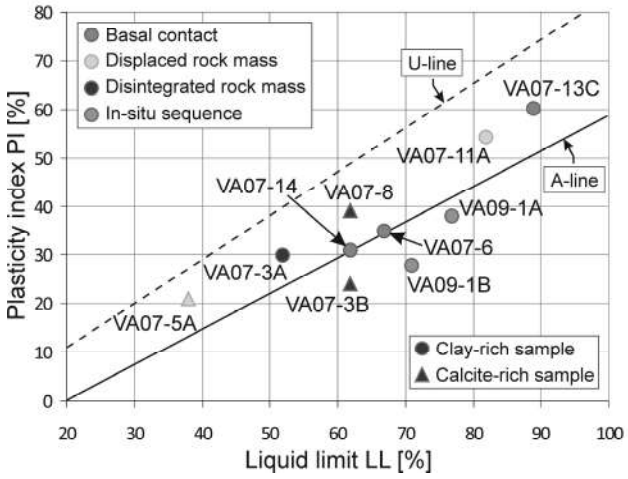

Fig. 13 1200 dpi. Plasticity chart of some selected clay samples exhumed from different geological contexts related to the Vajont landslide (modified from Bolla et al., 2020).

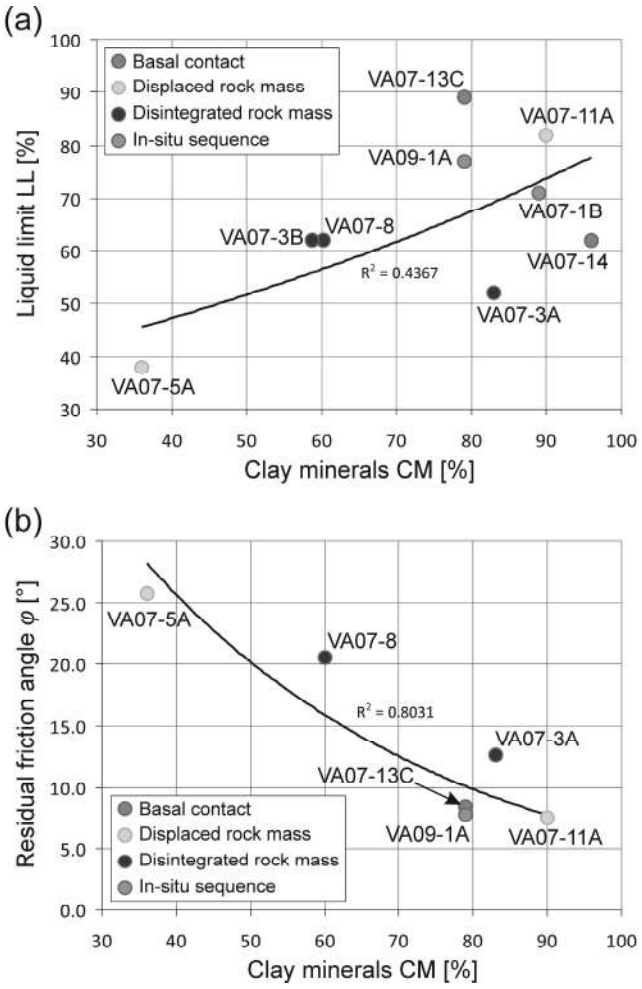

Fig. 14 1200 dpi. Correlation diagrams of some Vajont clay samples exhumed from different geological contexts, showing (a) liquid limit vs. clay mineral content and (b) residual friction angle vs. clay mineral content.